Rydberg-valence interactions of CO, and spectroscopic evidence characterizing the $C'\,^1\Sigma^+$ valence state

Michèle Eidelsberg and Françoise Launay
Observatoire de Paris, section de Meudon, LERMA, UMR 8112 du CNRS, 92195 Meudon Cedex, France

Kenji Ito and Takashi Matsui[a)]
Photon Factory, Institute of Materials Structure Science, High Energy Accelerator Research Organization, 1-1 Oho, Tsukuba, Ibaraki 305-0801, Japan

Paul C. Hinnen,[b)] Elmar Reinhold, and Wim Ubachs
Laser Center, Department of Physics and Astronomy, Vrije Universiteit, De Boelelaan 1081, 1081 HV Amsterdam, The Netherlands

Klaus P. Huber[c)]
Steacie Institute for Molecular Sciences, National Research Council of Canada, 100 Sussex Drive, Ottawa, Ontario K1A 0R6, Canada

(Received 17 February 2004; accepted 7 April 2004)

Rotationally cold absorption and two-photon ionization spectra of CO in the 90–100 nm region have been recorded at a resolution of 0.3–1.0 cm^{-1}. The analyses of up to four isotopomers seek to clarify the observations in regions where the Rydberg levels built on the ground state $X\,^2\Sigma^+$ of the ion interact with valence states of $^1\Sigma^+$ and $^1\Pi$ symmetry. Previous observations of the $3s\sigma$, $B\,^1\Sigma^+$ Rydberg state, reviewed by Tchang-Brillet *et al.* [J. Chem. Phys. **96**, 6735 (1992)], have been extended to energies above its avoided crossing with the repulsive part of the $D'\,^1\Sigma^+$ valence state where resonances of varying intensities and widths have been attributed to the fully coupled $3s\sigma$ or $4s\sigma$ and D' potentials, and where the B state approaches a second avoided crossing with the $C'\,^1\Sigma^+$ valence state [Cooper and Kirby, J. Chem. Phys. **87**, 424 (1987); **90**, 4895 (1989); Chem. Phys. Lett. **152**, 393 (1988)]. Fragments of a progression of weak and mostly diffuse bands, observed for all four isotopomers, have been assigned to the $C'\leftarrow X$ transition. The least-squares modeling of the $4p$ and $5p$ complexes reveals the $3p\pi$, $E\,^1\Pi$ Rydberg state to be one of the perturbers, violating the $\Delta v=0$ selection rule for Rydberg–Rydberg interactions on account of its rapid transition with increasing v from Rydberg to valence state. A second $^1\Pi$ perturber, very loosely bound and clearly of valence type, contributes to the confusion in the published literature surrounding the $5p$, $v=0$ complex. © *2004 American Institute of Physics.*
[DOI: 10.1063/1.1756579]

I. INTRODUCTION

Ever since Letzelter *et al.*[1] showed the photodestruction of CO to occur primarily at energies above 100 000 cm^{-1} (12.4 eV), with the dissociation process dominated by discrete rather than continuous absorption, renewed efforts have been made to refine the early analyses of the CO absorption spectrum by Ogawa and Ogawa[2,3] and to apply modern high resolution techniques to the study of the many interactions that shape the rovibronic structure at energies where the Rydberg series built on the $X\,^2\Sigma^+$ ion core converge to the first ionization potential[4–8] at 113 027.5±0.3 cm^{-1}.

Ten years prior to the study by Letzelter *et al.*,[1] Casey[9] had already undertaken detailed rotational analyses of a large number of absorption features in the 80–120 nm regions of $^{12}C^{16}O$ and $^{13}C^{16}O$. Apart from room temperature spectra, Casey had at his disposal rotationally cold spectra, all of them photographically recorded at the National Research Council in Ottawa using a 10 m grating spectrograph[10] with an estimated resolution of 0.7 cm^{-1}. This unpublished work has significantly contributed to a more recent review by Eidelsberg and Rostas[11] of absorption and photodissociation data for the four main isotopomers of CO. The effective parameters for many of the CO states are now fairly well established, owing primarily to the work of Ebata *et al.*[4,7,12,13] who use state specific triple-resonant photoionization and ion dip methods to probe higher members in the *s*, *p*, *d*, and *f* series from the $3s\sigma$, $B\,^1\Sigma^+$ or $3p\sigma$, $C\,^1\Sigma^+$ lowest Rydberg states of CO. The Rydberg levels are, however, not without anomalies. Frequently, molecular constants and isotope shifts are found to be incompatible with expectations based on the parameters of the ion core, and the Rydberg←Rydberg transitions tend to violate not only the one-electron atomic selection rule $\Delta l=\pm 1$, but also the selection rule $\Delta v=0$ that

[a)]Present address: Hydrotreating Catalysis Group, Research Institute for Green Technology, National Institute of Advanced Industrial Science and Technology (AIST), Tsukuba Central 5, 1-1-1 Higashi, Tsukuba, Ibaraki 305-8565, Japan.
[b)]Present address: ASM Lithography, De Run 6501, 5504 DR Veldhoven, The Netherlands.
[c)]Author to whom correspondence should be addressed. Electronic mail: klaus.huber@nrc-cnrc.gc.ca

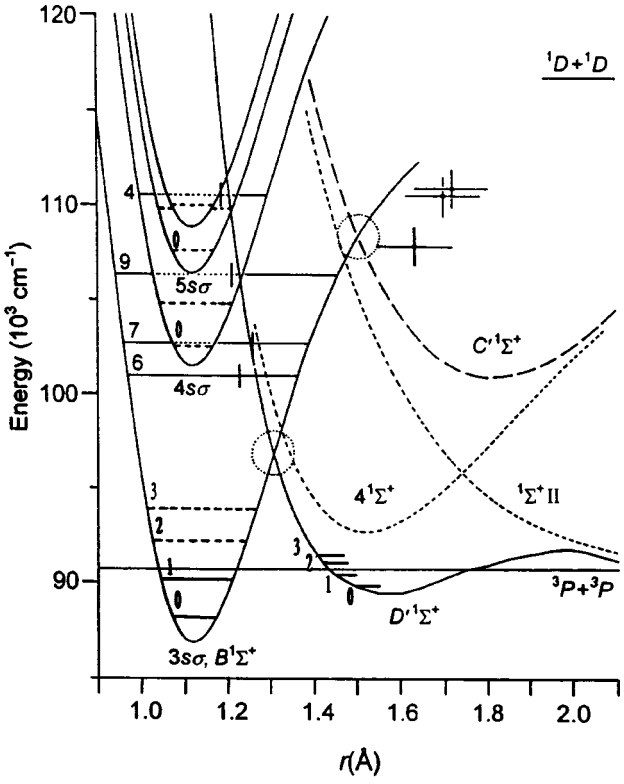

FIG. 1. Diabatic potentials of the $ns\sigma$ Rydberg states converging to $X\,^2\Sigma^+$ of CO^+ and of the interacting valence states $D'\,^1\Sigma^+$ and $C'\,^1\Sigma^+$ (adapted from Fig. 1 of Ref. 18). Energies are relative to the minimum of the neutral ground state. The *ab initio* calculated $4\,^1\Sigma^+$ and $^1\Sigma^+$II curves (see Sec. III B) have been used, in conjunction with D', to construct the approximate C' potential. Short vertical bars indicate the internuclear distances of selected $3s\sigma$ and $4s\sigma$ levels. Crosses mark the energies and r values of four C' levels.

ought to govern the transitions from the B and C states to Rydberg levels built on the same ion core.

The most striking aspect of the absorption spectrum is the diffuseness of many of its features. Line widths vary in seemingly random fashion from one band to the next and are strongly affected by isotopic substitution. *Ab initio* studies by Cooper and Kirby[14–16] suggest that this behavior, like the anomalies mentioned in the previous paragraph, has its origin in widespread interactions of the lowest Rydberg states with valence configurations. Because of their large internuclear distances, the valence states are not readily accessible from the neutral ground state. The one exception is the $\ldots 1\pi^3 5\sigma^2 2\pi$, $D'\,^1\Sigma^+$ state, shown in Fig. 1, which has been characterized by Wolk and Rich[17] from ultraviolet (UV) laser induced fluorescence studies of vibrationally excited CO. Tchang-Brillet *et al.*[18,19] were able to show that the interaction with the repulsive part of the weakly bound D' potential accounts for large changes to the vibrational and rotational parameters of the $3s\sigma$, $B\,^1\Sigma^+$ Rydberg state and for the increasingly large predissociation widths of its $v=2$ and 3 levels. At energies above 99 000 cm^{-1}, the strong coupling of the B and D' potentials leads to the appearance in absorption of $^1\Sigma^+$ resonances that are distinguished by widely varying intensities and line widths. Three such levels, observed in the spectra of four isotopomers, will be discussed in Sec. III A. The perturbations persist in higher members of the $ns\sigma$ series where the interactions are expected to scale according to $n^{-3/2}$.

The D' state displays a potential maximum at $r \approx 1.98$ Å[14] with a barrier height of close to 1048 cm^{-1} relative to the $^3P+^3P$ dissociation limit at 89 592 cm^{-1}.[18] It is considered[17] to be the product of a strongly avoided crossing of a bound $^1\Sigma^+$ state[20] arising from the $^1D+^1D$ limit by a purely repulsive[21] or only slightly bound state[22] of the same symmetry from $^3P+^3P$ ground-state products. The second adiabatic potential resulting from the interaction is most likely the *ab initio* predicted $C'\,^1\Sigma^+$ state of Cooper and Kirby.[14] The calculations[14,23] place its minimum at about 107 600 cm^{-1} above the minimum of the CO ground state and predict an internuclear distance of close to 1.8 Å. In the 106 600–110 400 cm^{-1} region of four isotopomers, we identify fragments of a progression of strongly red shaded and mostly diffuse $^1\Sigma \leftarrow {}^1\Sigma$ bands which seem to support the expectations. Section III B links the upper-state levels of the bands to the C' potential, pointing out similarities with the A states of the alkali hydrides[24] which also represent the upper adiabatic component of an avoided crossing of a strongly bound state by a repulsive potential from ground-state products. The analysis shows the *ab initio* calculations to underestimate the depth of the C' potential, possibly by as much as 5400 cm^{-1}.

Section III C investigates the low-n p complexes at energies between 103 000 and 109 600 cm^{-1}. The $4p(v=0)$ complex with its σ component at 103 054 cm^{-1} has been described before.[25] Here, we resume the modeling of this complex and of the alleged $3d\pi(v=1)$ level long noted[9,11] for its anomalously small rotational constant, assuming both Π levels to interact with one $^1\Pi$ perturber of mixed Rydberg-valence type. The $5p(v=0)$ and $4p(v=2)$ complexes at 107 174 and 107 366 cm^{-1} interact with two $^1\Pi$ perturbers, one diffuse and clearly of valence type, the other of mixed character and resembling the perturber involved with $4p\pi(v=0)$ and $3d\pi(v=1)$. The result is a very complex spectrum that has lead to conflicting band assignments by earlier investigators.[9,11] Finally, the narrow interval from 109 300 to 109 600 cm^{-1} contains transitions to $4p(v=3)$ and $5p(v=1)$,[25] the σ component of the former interacting with a bright $^1\Sigma^+$ level assumed to have mixed $4s\sigma \sim D'\,^1\Sigma^+$ character. Also involved is a dark $^1\Pi$ state of unknown origin.

Considerable confusion rules the labeling of the singlet Rydberg states of CO. Some authors adhere to the familiar custom of using capital letters, others prefer the *ad hoc* number indices from Refs. 1 and 11, or they chose a combination of the two schemes. We retain the letters B, C, and E for the $3s\sigma$, $3p\sigma$, and $3p\pi$ lowest Rydberg states. For *deperturbed* levels of higher n, we prefer the notation $X^+(v)nl\lambda$ or $A^+(v)nl\lambda$ adopted from Ref. 26 and now well established for Rydberg states of the N_2 molecule.[27] A shorter notation, $nl\lambda(v)$ or $nl(v)$, may also be used. The observed *perturbed* vibronic levels included in a least-squares fit will be referred to by their symmetry, numbered in order of increasing energy $(1\,^1\Sigma^+, 2\,^1\Sigma^+ \cdots 1\,^1\Pi, 2\,^1\Pi \ldots)$.

II. EXPERIMENT

Rotationally cold absorption spectra in the 87.5–111.0 nm region of four CO isotopomers (12–16, 13–16, 12–18, 13–18) have been photographically recorded on Kodak SWR plates using the pulsed supersonic free jet expansion installed at the 10.6 m vacuum ultraviolet (VUV) spectrograph of the Observatoire de Paris in Meudon.[25] The background continuum was emitted from a three-electrode vacuum spark appropriately synchronized with the pulsed jet expansion. With a 30 μm slit, and working in first order of a holographic normal-incidence concave grating having 3600 lines/mm, we achieved a resolution of marginally better than 1 cm^{-1}. The rotational temperature of weak bands was estimated at around 10–20 K, the uncertainty being greater for strong transitions, which tend to exhibit tails of high-J lines owing to absorption by warmer CO gas along the light path of the experiment. The spectra, measured against Cu II lines recorded in the same order, have been calibrated with the help of the Ar resonance lines at 104.821 99 and 106.665 99 nm and N_2 impurity lines of known wavelengths.[28] We have also made use of room temperature spectra recorded earlier[11] under equilibrium conditions.

Photographic jet absorption spectra for the main isotope were also recorded using a continuous jet expansion at the 6.65 m VUV spectrograph[29] on beamline 12-B of the Photon Factory synchrotron facility in Tsukuba. Details regarding the interfacing of the jet expansion with the synchrotron radiation may be found in Ref. 30. Taking advantage of the zero-dispersion order sorter described by Ito *et al.*,[29] and using a slit width of 10 μm, we recorded the spectra in the sixth order of a 1200 lines/mm concave grating at a resolution of $\sim$0.5 cm^{-1}. They were measured against CO fourth positive emission lines recorded in the overlapping third order. Where well-defined lines can be compared with calibrated two-photon ionization measurements,[31] the required corrections turn out to be of the order of $+0.40$ cm^{-1}. Other data are used without correction.

Information complementary to the photographic data comes from resonance enhanced two-photon ionization spectra recorded in 1993 and 1995 at the Laser Center of the Vrije Universiteit in Amsterdam. The VUV laser setup and its application to spectroscopic studies of CO has been described by Eikema *et al.*[31] Very briefly, the coherent VUV radiation is produced by nonlinear upconversion of the visible output from a tunable dye laser using frequency doubling in a crystal and subsequent frequency tripling of the generated UV light in a pulsed ($\sim$10 Hz) rare-gas jet. The VUV light crosses a skimmed CO jet at right angles, exciting the CO molecules to a Rydberg level from where they are transferred to the ionization continuum by the powerful UV light that overlaps the VUV beam both spatially and temporally. The resulting 1VUV+1UV signal is registered by detecting the time-of-flight mass selected CO^+ ions. The VUV band width is close to 0.30 cm^{-1}, increasing slightly with decreasing wavelength to 0.44 cm^{-1} at 90.5 nm,[32] the shortest wavelength attainable with the frequency doubled Nd:YAG pump laser. The visible output of the dye laser at its fundamental frequency is used for on-line calibration of the VUV spectra against iodine standards;[33] the absolute accuracy of the CO line wave numbers is estimated at ± 0.13 cm^{-1}.[31] Finally, the rotational temperature of the two-photon ionization spectra can be controlled by varying the stagnation pressure of the CO jet expansion, the distance of the nozzle orifice from the interaction region, and/or the time delay settings.

III. RESULTS AND DISCUSSION

The observed R, Q, and P branch transitions, properly weighted, have been fitted to transition energies calculated from the known ground state constants of CO[34,35] and from the eigenvalues of simple Hamiltonian matrices which model the Rydberg complexes and their interactions with the perturber states. The diagonal matrix elements,

$$\langle n,v,\Lambda|H_{ev}+H_r|n,v,\Lambda\rangle = T_v + B_v[J(J+1)-\Lambda^2] - D_v[J(J+1)-\Lambda^2]^2, \quad (1)$$

are complemented by off-diagonal elements representing the homogeneous interactions with the perturbers,

$$\langle n,v,\Lambda|H_{ev}|n',v',\Lambda\rangle, \quad (2)$$

and the l uncoupling interaction between the e levels of a p complex,

$$\langle n,v,l,\Lambda,e|H_r|n,v,l,\Lambda\pm 1,e\rangle = -B_v[2l(l+1)]^{1/2}[J(J+1)]^{1/2} = -\alpha[J(J+1)]^{1/2}. \quad (3)$$

The Λ-type doubling of the $^1\Pi$ perturbers, before allowing for their interactions with the Rydberg levels, is assumed to be negligibly small. Also, the homogeneous interactions between Rydberg levels built on the same core, but differing in the vibrational quantum number v, are expected to be very small and will be neglected for the purpose of this work.

Most of the line wave numbers and term values treated in the following sections have been collected in Tables A-I to A-VI of an unpublished Appendix to this paper. They have been deposited with the Electronic Physics Auxiliary Publication Service (EPAPS) of the American Institute of Physics.[36] Copies are also available from one of the authors (K.P.H.).

A. Levels of mixed $B\,^1\Sigma^+ \sim D'\,^1\Sigma^+$ character

Tchang-Brillet *et al.*[18,19] have applied nonperturbative close coupling methods to the modeling of the interaction of the $3s\sigma$, $B\,^1\Sigma^+$ Rydberg with the repulsive $D'\,^1\Sigma^+$ valence state. At energies below the crossing of the diabatic potential curves, they find good agreement of the calculated with the observed level shifts, relative band intensities, and predissociation widths. Extrapolations of the calculations[37] to energies above the crossing foresee large variations in these quantities for resonances which, instead of being associated with one state or the other, relate to the fully coupled potentials of both states. A treatment by Atabek and Lefebvre[38] of an avoided crossing of an attractive by a repulsive state of Se_2 comes to similar conclusions. Here, we report observations on three B state levels of strongly mixed Rydberg-

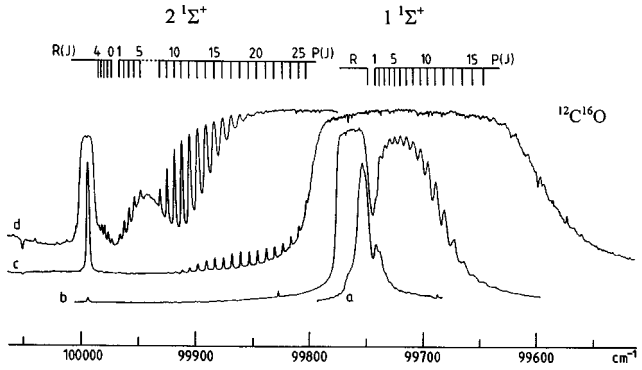

FIG. 2. Jet and room temperature absorption spectra of transitions to two $^1\Sigma^+$ levels arising from the interaction of $B(6)$ and $X^+(0)3d\sigma$ of $^{12}C^{16}O$. (a) Jet absorption spectrum; (b)–(d) room temperature spectra recorded with a path length of ~20 m at CO pressures of 5×10^{-4}, 5×10^{-3}, and 1.5×10^{-1} Torr.

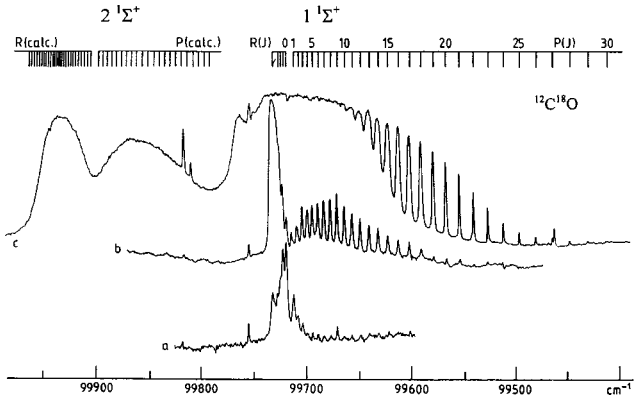

FIG. 3. Jet and room temperature absorption spectra of transitions to two $^1\Sigma^+$ levels arising from the interaction of $B(6)$ and $X^+(0)3d\sigma$ of $^{12}C^{18}O$. (a) Jet absorption spectrum; (b) and (c) room temperature spectra recorded with a path length of ~20 m at CO pressures of 10^{-4} and 3×10^{-3} Torr.

valence type at energies above the avoided crossing. For simplicity, they will be identified by their Rydberg character only.

Casey[9] points out that a diffuse $^1\Sigma^+\leftarrow{}^1\Sigma^+$ band of $^{12}C^{16}O$ near 99 745 cm^{-1}, tentatively assigned by Ogawa and Ogawa[3] to $X^+(0)3d\sigma$, is accompanied by a sharper and weaker $^1\Sigma^+\leftarrow{}^1\Sigma^+$ transition at 99 970 cm^{-1}, and that the upper states are coupled by a matrix element of 112 cm^{-1}. Figure 2 reproduces the spectrum of $^{12}C^{16}O$. The stronger band of lower energy displays a clear zero gap in the jet absorption spectrum of trace *a*, and the room temperature spectrum of trace *b* reveals a series of broad *P* branch lines, their intensities reaching a maximum for $P(6)$ or $P(7)$ before rapidly falling off for higher rotation. At the tenfold increased pressure of trace *c*, considerably narrower lines of high *J* begin to appear in the *P* branch of the weaker band, together with a linelike feature at 99 994.4 cm^{-1} that contains the corresponding high-*J* *R* lines. In trace *d*, finally, with the pressure increased by yet another factor of 30, the *P* and *R* lines of the weaker band can be followed right down to the zero gap, except for $P(6)$ and $P(7)$ which seem to be absent. The very different relative intensities of the bands, as well as the prevalence of high-*J* over low-*J* transitions in the less saturated band at 99 970 cm^{-1}, are readily understood (see, e.g., Ref. 39) in terms of transition amplitudes from the $X\,^1\Sigma^+(v=0)$ ground state to two interacting $^1\Sigma^+$ levels which the deperturbation shows to be mixtures of $B(6)$ and $X^+(0)3d\sigma$, the former having substantial D' character. The observed amplitudes arise from constructive and destructive interference of the unperturbed and nearly equal amplitudes in the bands of lower and higher energies, respectively, strengthening the former at the expense of the latter whose *P* branch lines are seen to disappear at around 99 940 cm^{-1} for rotational quantum numbers close to the crossing of the unperturbed levels.

Figure 3 reproduces the corresponding bands of $^{12}C^{18}O$. The discrete structure is confined to the band of lower energy, and the band of higher energy appears as a broad continuum with *P* and *R* branch maxima at ~99 865 and 99 935 cm^{-1}. Similar spectra were recorded for the 13–16 isotopomer. The diffuse peak near 99 935 cm^{-1} of trace *c*, recorded at a pressure of 3×10^{-3} Torr, is also seen in trace *d* of Fig. 2 where it arises from absorption by the 12–18 and 13–16 isotopomers in natural abundance at a combined partial pressure of 2×10^{-3} Torr.

With the help of low temperature spectra, the assignment of rotational quantum numbers is straightforward, except for $^{13}C^{16}O$ where the input data consist of a small group of low-*J* jet absorption lines and a series of unrelated high-*J* *P* lines from room temperature spectra. The correct numbering of the latter was established by systematically changing the assigned *J* values in search for the best fit of the calculated to the observed line wave numbers.

Term values for the two interacting $^1\Sigma^+$ states of three isotopomers are collected in Table A-I.[36] Figure 4 displays the reduced terms for $^{12}C^{16}O$. The deperturbed levels $B(6)$ and $X^+(0)3d\sigma$ are calculated with parameters from Table I, taking into account the *l* uncoupling interaction of the σ with the π component[3] of the $3d$ complex. For the main isotope, the deperturbed terms cross between $J=7$ and 8, close to predictions made from the disappearance of $P(6)$ and $P(7)$ in the band at 99 970 cm^{-1}.

The molecular parameters in Table I, together with the quantum defect of 0.1160, unambiguously identify the deperturbed $^1\Sigma^+$ level at 99 846 cm^{-1} as $X^+(0)3d\sigma$. The $B(6)$ level at 99 868 cm^{-1} with an effective *B* value of only 1.6376 cm^{-1} fits expectations for a level of mixed $B\sim D'$ character. Its internuclear distance of ~1.23 Å is close to the crossing of the diabatic potential curves[18] at 1.31 Å, suggesting that the radial wave function is concentrated, very roughly, in the region of the well formed by the upper adiabatic curve. The choice of $v=6$ comes from a comparison with the vibrational levels calculated for a *B* state potential identical to that of the $X\,^2\Sigma^+$ ion core and with its minimum fixed at $T_e=86\,926.9$ cm^{-1}.[40] The $v=6$ level, deperturbed from the interaction with $3d\sigma(0)$, but not with $D'\,^1\Sigma^+$, is found to be at 271 cm^{-1} above its calculated energy of 99 597 cm^{-1}.

A very weak band consisting of narrow lines, which are readily assigned to a strongly red shaded *R* and its corresponding *P* branch, appears at 101 556 cm^{-1} of the $^{12}C^{16}O$ spectrum on the shortward wing of the much stronger and very diffuse $X^+(0)4s\sigma$ band. Ogawa and Ogawa[3] describe

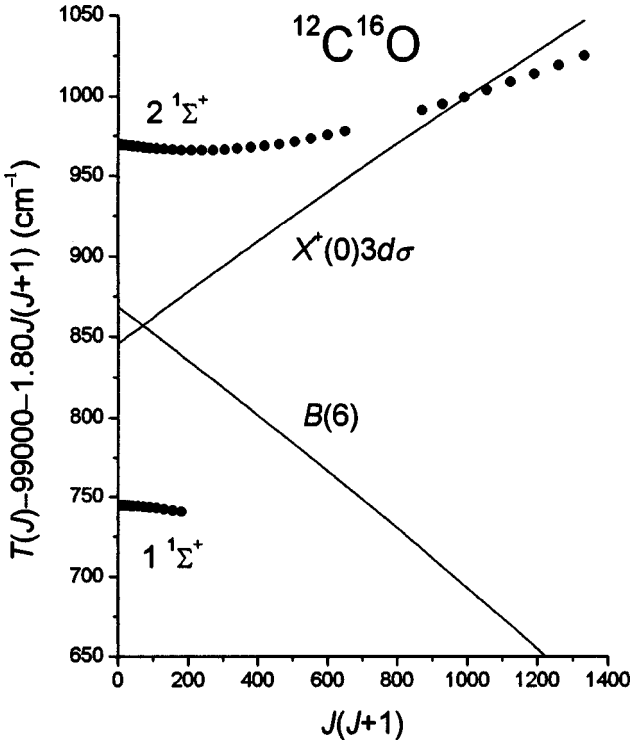

FIG. 4. Reduced observed (full circles) and deperturbed term values (solid lines) for the interacting $B(6)$ and $X^+(0)3d\sigma$ levels of $^{12}C^{16}O$. The deperturbation takes into account the l uncoupling interaction of the σ with the π component of $3d$.

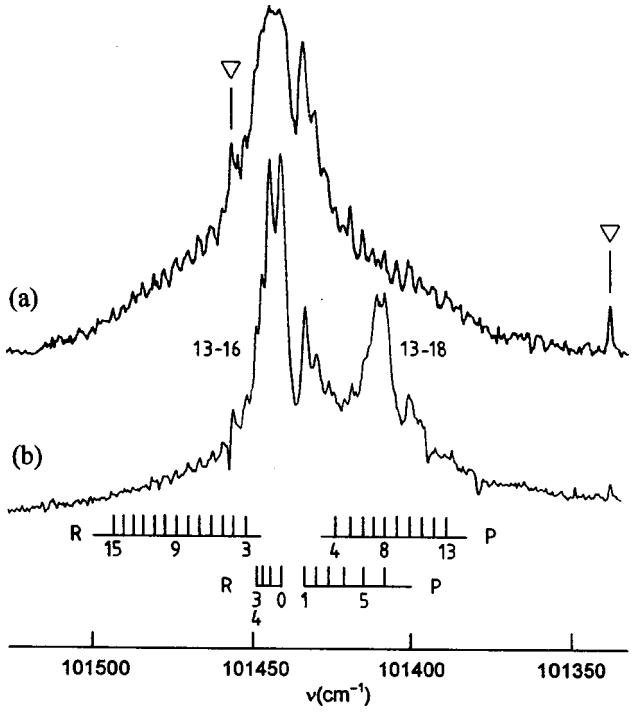

FIG. 5. Jet absorption spectra of the $X^+(0)4s\sigma \leftarrow X(0)$ transition of $^{13}C^{16}O$. The upper-state levels near $J=3$ are weakly perturbed by $B(7)$. Two impurity lines, marked by triangles in trace (a), represent the $R(1)$ and $Q(1)$ lines of the $C \leftarrow X$ 1–0 band of H_2 at 101 456.50 and 101 337.89 cm^{-1}. The spectrum of trace (b) contains a $^{13}C^{18}O$ impurity.

this feature as linelike. Casey[9] reports the $Q(1)$ line, an observation we do not confirm. This $^1\Sigma^+$ upper state is also seen from $B(0)$ at 14 640 cm^{-1} of the $C(^3P)$ photofragment spectrum [see Fig. 3(a) of Ref. 41]. We assign it as $B(7)$ on the basis of its energy at 1688 cm^{-1} above $B(6)$ and at only 43 cm^{-1} below its calculated energy. The effective B value of 1.543 cm^{-1} and $r=1.26$ Å are compatible with expectations for a level of mixed $B \sim D'$ character.

The corresponding transition of $^{13}C^{16}O$ is hidden inside the diffuse, though partly resolved, $X^+(0)4s\sigma$ band reproduced in Fig. 5. The line assignments in the lower part of the figure emerged from a careful search for known ground-state combination differences. Figure 6 shows the crossing of the $4s\sigma(0)$ and $B(7)$ rotational levels at $J=3$ to be weakly avoided with a matrix element of 1.3 cm^{-1}. In $^{12}C^{18}O$, the $B(7)$ perturber has shifted to lower energies, leaving no signs of an interaction with $4s\sigma(0)$. The rovibronic term values and derived molecular parameters for all three isotopomers can be found in Table II where, incidentally, the rotational constants for $X^+(0)4s\sigma$ are seen to be substantially smaller than $B=1.8810$ or 1.8738 cm^{-1} for the 13–16 or

TABLE I. The homogeneous interaction of $B(6)$ with $X^+(0)3d\sigma$ of CO. The parameters (cm^{-1}) for three isotopomers derive from nonlinear least-squares fits to the observed R and P branch transitions. Adjusted parameters are given with 1σ error limits (in parentheses) in units of the last-quoted decimal place. Other parameters were kept fixed at their estimated values.

		12–16	13–16	12–18
$B(6)$	T_6	99 868.38(29)	99 792.2(6)	99 787.44(32)
	B_6	1.6376(12)	1.5646(8)	1.558 04(33)
	$D_6\times10^5$	1.4(8)	1.0	1.0
$X^+(0)3d\sigma$	T_0	99 845.78(30)	99 835.1(11)	99 834.99(37)
	B_0	1.9611(24)	1.8809	1.8738
	$D_0\times10^5$	0.81(11)	0.57	0.57
$X^+(0)3d\pi$	T_0	101 032.82(7)[a]	101 030.0	101 030.0
	B_0	1.9233(9)[a]	1.8809	1.8738
	$D_0\times10^5$	0.75(20)[a]	0.57	0.57
$\langle B(6)\|H_{ev}\|X^+(0)3d\sigma\rangle$		111.956(19)	91.4	91.42(12)
$\langle X^+(0)3d\sigma\|H_r\|X^+(0)3d\pi\rangle$		6.82[b]	6.52[b]	6.49[b]
σ_{fit}		0.16	0.12	0.12

[a]Term values for e parity levels derived from data in Ref. 3.
[b]J-independent electronic factor α of the matrix element [Eq. (3)].

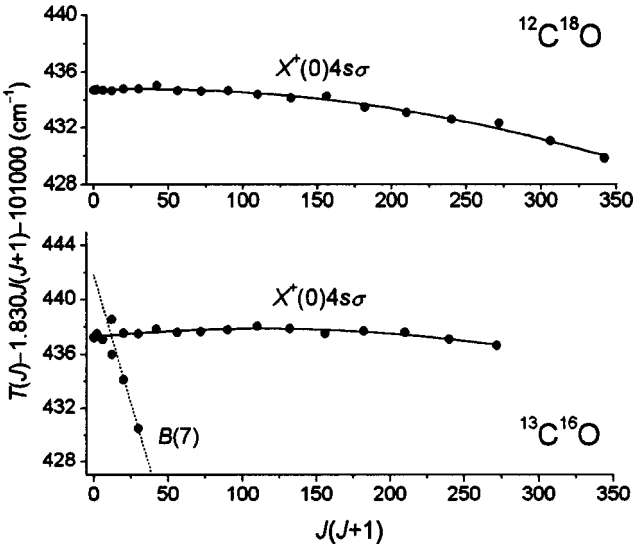

FIG. 6. Reduced term values for $X^+(0)4s\sigma$ and $B(7)$ of $^{13}C^{16}O$ and $^{12}C^{18}O$. Full circles and solid lines refer to the observed and recalculated data, respectively.

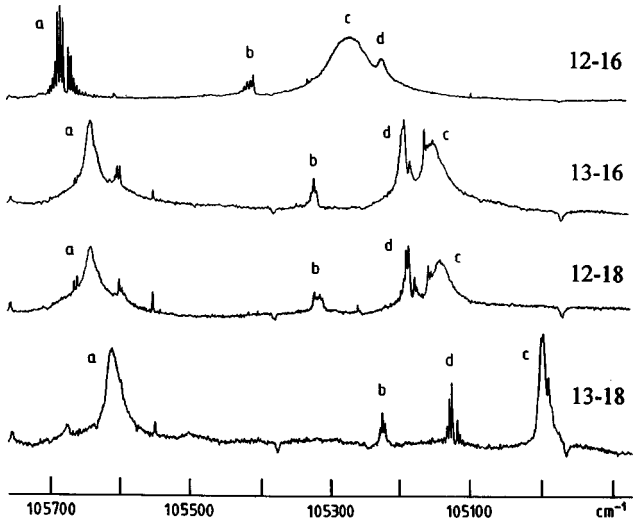

FIG. 7. Absorption spectra of four CO isotopomers in the 104 900–105 700 cm^{-1} region. The transitions to $X^+(0)4d\sigma$, $X^+(1)4p\pi$, $B(9)$ and $X^+(1)4p\sigma$ are labeled *a*, *b*, *c*, and *d*, respectively.

12–18 ion core, a sure sign that $X^+(0)4s\sigma$, too, mixes with $D'\,^1\Sigma^+$.

Figure 7 reproduces the jet absorption spectra of four isotopomers in the region from 104 900–105 700 cm^{-1}. Of two structureless features seen at 105 268 and 105 219 cm^{-1} of the $^{12}C^{16}O$ spectrum, labeled *c* and *d*, Casey[9] convincingly identified the weaker and narrower band *d* with the transition to $X^+(1)4p\sigma$, arguing that its separation from the well established 0–0 band at 103 055 cm^{-1} as well as its isotope shift and upper-state *B* value in $^{13}C^{16}O$ are all very close to expectations for a Rydberg level built on $X\,^2\Sigma^+$, $v=1$. Additional confirmation comes from the 12–18 and 13–18 parameters in Table III.

TABLE II. The $B(7)\sim X^+(0)4s\sigma$ interaction of CO; term values and molecular parameters (cm^{-1}). Numbers in parentheses give the differences obs−calc for levels used in the least-squares fit, or 1σ error limits for the derived parameters, both in units of the last-quoted decimal place.

	12–16 $B(7)$	13–16 $B(7)\sim X^+(0)4s\sigma$		12–18 $X^+(0)4s\sigma$
J	$T(J)$	$T(J)$	$T(J)$	$T(J)$
0	101 556.0(−1)	101 437.23(−3)		101 434.69(−1)
1	101 559.2(0)	101 441.13(+19)		101 438.38(+2)
2	101 565.2(−2)	101 448.05(−25)		101 445.65(−4)
3	101 574.6(0)	101 457.94	101 460.52	101 456.60(−9)
4	101 586.6(−3)	101 470.69	101 474.14(+9)	101 471.36(+2)
5	101 602.3(−1)	101 485.38	101 492.40(−3)	101 489.68(+3)
6	101 621.5(+7)		101 514.69(+21)	101 511.89(+29)
7	101 642.5(+1)		101 540.06(−12)	101 537.11(−9)
8	101 667.2(+2)		101 569.40(−13)	101 566.37(−6)
9	101 694.7(+1)		101 602.47(−5)	101 599.32(+4)
10	101 725.1(−2)		101 639.32(+18)	101 635.66(−9)
11	101 758.8(−2)		101 679.43(+5)	101 675.67(−14)
12	101 795.5(−2)		101 722.98(−25)	101 719.70(+23)
13	101 835.2(−2)		101 770.71(+3)	101 766.50(−20)
14	101 878.4(+3)		101 821.86(+16)	101 817.34(−14)
15			101 876.27(−1)	101 871.76(−5)
16			101 934.36(−5)	101 930.08(+42)
17				101 991.02(0)
18				102 055.71(−15)
T_v	101 556.10(13)	101 441.8[a]	101 437.26(8)[b]	101 434.70(7)
B_v	1.5432(36)	1.453[a]	1.8404(16)[b]	1.8332(13)
$D_v\times10^5$	4.7(18)		4.66(61)[b]	4.94(39)
		$\langle B(7)\|H_{ev}\|4s\sigma(0)\rangle\approx1.3$		
$\sigma_{\rm fit}$	0.27		0.16	0.17

[a]Parameters for $B(7)$, estimated from its deperturbed $J=3$ and observed $J=5$ levels (see Fig. 6).
[b]Parameters for $X^+(0)4s\sigma$.

TABLE III. Rovibronic term values and molecular parameters (in cm^{-1}) from jet absorption data for $B(9)$ and $X^+(1)4p\sigma$ of four CO isotopomers; residuals obs−calc and 1σ error limits (both in parentheses) are given in units of the last-quoted decimal place.

	J	12–16	13–16	12–18	13–18
$B(9)$	0	105 268[a,b]	105 150[a,b,c]	105 140.7[a,b,d]	104 995.93(−11)[b]
	1				104 999.26(+18)
	2				105 005.12(−5)
				T_9	104 996.04(18)
				B_9	1.52(5)
				σ_{fit}	0.21
$X^+(1)4p\sigma$	0	105 219[a]	105 186.21(−10)	105 180.71(−10)	105 125.78(+1)
	1		105 190.04(+16)	105 184.57(+3)	105 129.37(+3)
	2		105 196.97(−5)	105 192.24(+23)	105 136.41(−7)
	3			105 203.08(−13)	105 147.23(+3)
	4			105 218.00(−14)	105 161.8
	5			105 236.90(+9)	
		T_1	105 186.31(16)[e]	105 180.81(10)	105 125.77(4)
		B_1	1.79(5)[e]	1.867(6)	1.786(6)
		σ_{fit}	0.20[e]	0.16	0.06

[a]Maximum of continuous absorption.
[b]Rotational line widths are estimated to be of the order of 50–70 cm^{-1} for $^{12}C^{16}O$ and 2–5 cm^{-1} for $^{13}C^{18}O$, with intermediate values for the other two isotopes.
[c]Overlapped by discrete features at 105 161.48, 105 157.51, 105 154.2, 105 149.61 cm^{-1}.
[d]Overlapped by discrete features at 105 156.73 and 105 153.03 cm^{-1}.
[e]Casey's data (Ref. 9), obtained under equilibrium conditions, reduce for $J=1-8$ to $T_1=105\,186.27(10)$, $B_1=1.8628(26)$, $\sigma=0.17\ cm^{-1}$; data for $J=0$, 9, and 10 may be based on misassigned and/or perturbed lines.

The stronger and broader band *c* is more difficult to assign. For $^{13}C^{18}O$, its rotational structure is just barely resolved; it confirms the $^1\Sigma^+$ symmetry of the upper state and suggests a B value of $\sim 1.52\ cm^{-1}$ and an internuclear distance in the neighborhood of 1.21 Å, again favoring the assignment to a $B\sim D'$ mixed level. The most likely choice is $B(9)$, based on a short extrapolation from $B(6)$ and $B(7)$. The $B(9)$ level of $^{12}C^{16}O$ is observed at 243 cm^{-1} below the calculated term of 105 511 cm^{-1}.

The shifts of the observed relative to the calculated $B\,^1\Sigma^+$ levels, reported above for $v=6$, 7, and 9, correspond to the shifts δG_v established in Refs. 18 and 19 for energies below the crossing of the diabatic $B\,^1\Sigma^+$ and $D'\,^1\Sigma^+$ potentials. Figure 8 summarizes the results. The shifts above and below the crossing are seen to be of comparable magnitudes, though not necessarily of the same sign, creating a pattern that is reminiscent of the level shifts evaluated by Atabek and Lefebvre[38] for a similar interaction in the spectrum of Se_2.[42] At energies below the crossing, the shifts for all four CO isotopomers follow the same energy dependence, which is determined by the shape of the distorted *B* state potential curve. At higher energies, above the crossing, the shifts present a more complex pattern that cannot be rationalized in terms of a single potential curve.

Based on parameters derived by Tchang-Brillet *et al.*[18] from the modeling of the $B(v=0-2)\sim D'$ interaction, Andric *et al.*[37] used computational methods to predict the resonances arising from the fully coupled potentials at higher energies. A comparison of their Fig. 3 with Fig. 8 of the present work shows the levels $v=6$, 7, and 9 of $^{12}C^{16}O$, observed at 99 868, 101 556, and 105 268 cm^{-1} of the absorption spectrum, or at 14 023, 15 711, and 19 423 cm^{-1} relative to the *B* state minimum, to correspond, more or less, with resonances predicted at 14 713, 15 597, and 19 438 cm^{-1} but labeled $v=7$, 8, and 10. Irrespective of the disagreement concerning the vibrational numbering, the experimental and calculated energies for the first two resonances differ by −690 and +114 cm^{-1}, and the predicted predissociation widths for the second and third resonance are just the reverse of what is observed. The calculations of Andric *et al.*[37] are based on parameters which, although optimized for best representation of the $B\sim D'$ mixed levels from $v=0$ to 2 or 3,[18,19] are inadequate for long extrapolations to levels as high as $v=9$ or 10. Instead of adjusting the core

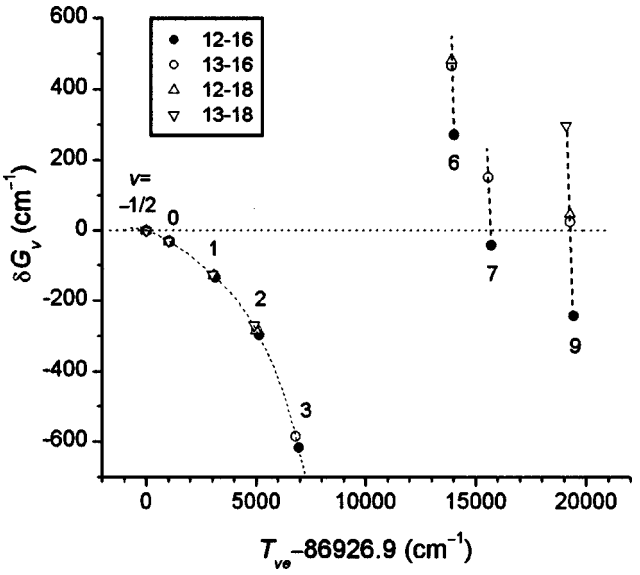

FIG. 8. The shifts δG_v of the observed relative to the calculated *B* state vibronic levels of four CO isotopomers below and above the crossing of the diabatic $B\,^1\Sigma^+$ and $D'\,^1\Sigma^+$ potentials (see text). On the scale of the figure, the crossing occurs at 9877.3 cm^{-1} (see Ref. 18).

parameters, it might be preferable not only to consider the interactions of the Rydberg levels with the $D'\,^1\Sigma^+$ valence state, but also to account for their mixing at higher energies with $C'\,^1\Sigma^+$ which shares with D' its origin from the same avoided crossing of a bound with a repulsive state. The following section reviews the experimental evidence concerning the C' valence state.

B. The $C'\,^1\Sigma^+$ valence state

Figure 1, presented already in Sec. I, displays the potential curves for the lowest four $ns\sigma$ states together with the D' and C' valence state potentials. The potential curves are shown in diabatic form, neglecting the fact that the crossings of the B state by the D' and, very likely, C' curves are strongly avoided. Also shown are the *ab initio* calculated potentials for two $^1\Sigma^+$ states whose avoided crossing is responsible for the formation of the D' and C' states. The bound $4\,^1\Sigma^+$ state of Cooper and Langhoff[20] is represented by a Morse potential calculated with the theoretical spectroscopic constants listed by these authors. The repulsive $^1\Sigma^+$II state is taken from Fig. 1 and Table VI of O'Neil and Schaefer.[21] Finally, the two *ab initio* calculated curves, in conjunction with the D' curve of Tchang-Brillet *et al.*,[18] were used to construct the C' potential. It crosses the $B\,^1\Sigma^+$ state at energies somewhere between 107 000 and 111 000 cm^{-1} where a number of previously unassigned levels appear in the absorption spectrum.

Casey[9] reports two diffuse and red shaded bands at 106 884 and 106 789 cm^{-1} in the spectra of $^{12}C^{16}O$ and $^{13}C^{16}O$, respectively, and Eidelsberg and Rostas,[11] confirming the observations, add the corresponding bands of $^{12}C^{18}O$ and $^{13}C^{18}O$ at 106 780 and 106 681 cm^{-1}. Three of these rather weak transitions can be seen in Fig. 12 of Sec. III C below where they appear, labeled *a*, just longward of the complex structures associated with the $5p(0)$ complex. The upper-state vibrational quantum number common to all four bands appears to be of moderate to high value.

The lines in the 13–16 and 12–18 bands at 106 789 and 106 780 cm^{-1} are narrow enough for unambiguous rotational assignments to be made. Both bands consist of strongly degraded R and P but no Q branches, showing the upper states to be of $^1\Sigma^+$ symmetry with very small rotational constants. The latter are reminiscent of the description by Komatsu *et al.*[13] of a $^1\Sigma^+$ level—in this instance of $^{12}C^{16}O$—observed at 20 440 cm^{-1} of the triple resonant ion-dip spectra from $v=1$ of $B\,^1\Sigma^+$. Term values and molecular parameters for the three rotationally analyzed $^1\Sigma^+$ levels are collected in Table IV.

A systematic search of the jet absorption spectra of four isotopomers reveals a small number of additional bands, all of them weak and narrow features of varying diffuseness. One band showing barely detectable rotational structure is reproduced in Fig. 9. The bands are generally free of overlapping features, the exception being a narrow continuum of $^{12}C^{16}O$ at 110 314 cm^{-1} which is blended with sharp structure arising from the much stronger transition to the $7p(0)$ complex. Table V summarizes the vibronic data. The vibrational intervals increase, rather than decrease, with increasing quantum number v. The anomaly is familiar from the spectra of the alkali hydrides[24] where the negative anharmonicity of the $A\,^1\Sigma^+$ first excited state can be traced to the unusual shape of the A state potential which, together with the ground state, results from an avoided crossing of a bound by a repulsive state. That the same anomaly is displayed by the four progressions of Table V lends some support for their assignments to the upper component of a similar avoided crossing. The vibrational constants for $C'\,^1\Sigma^+$, shown at the bottom of the table, were obtained from mass reduced plots of the observed energies T_{ve} versus $\rho(v+\frac{1}{2})$ by adjusting the integer x of the first column until the best fit of the calculated to the observed energies was found for $x=7$; ρ^2 is the ratio of the reduced masses, μ/μ_i. A rather long extrapolation establishes the C' potential minimum at $T_e \approx 102\,200$ cm^{-1}, or at ~5400 cm^{-1} below the *ab initio* calculated minima.[14,23] The vibrational frequency, $\omega_e = 718$ cm^{-1}, exceeds the *ab initio* result[14] by 20%.

The most puzzling aspect of the levels attributed to $C'\,^1\Sigma^+$ is their visibility from $v=0$ of $X\,^1\Sigma^+$. In Fig. 1, the energies and r values of the rotationally analyzed levels (Table IV and Fig. 9) are marked by four crosses, two of them overlapping each other. The internuclear separations are substantially shorter than the 1.91 or 1.83 Å predicted for the minima of the *ab initio* calculated C' potential curves.[14,23] They are, however, slightly longer than in the D' state which is inaccessible from $X\,^1\Sigma^+$ except in transitions from very highly excited vibrational levels.[17] In contrast, all

TABLE IV. Term values and molecular parameters (cm^{-1}) for three diffuse $^1\Sigma^+$ valence state levels of CO. Residuals obs−calc and 1σ error limits (in parentheses) are given in units of the last-quoted decimal place. Data for $^{12}C^{16}O$ derive from the triple-resonant ion-dip spectra of Ref. 13, with term values for $B\,^1\Sigma^+$, $v=1$ taken from Ref. 40.

J	12–16 $T(J)$	13–16 $T(J)$	12–18 $T(J)$
0	109 440.0(+23)		
1	109 437.0(−24)	106 790.9(+7)	106 782.16(−6)
2	109 442.5(−3)	106 794.6(+9)	106 785.82(+10)
3	109 447.5(−4)	106 798.5(−5)	106 791.03(+8)
4	109 455.5(+7)	106 806.0(−0)	106 797.66(−27)
5	109 464.0(+7)	106 814.6(−2)	106 806.64(−2)
6	109 473.0(−6)	106 825.2(−2)	106 817.18(+5)
7		106 837.6(−1)	106 829.30(−3)
8		106 851.5(−2)	106 843.27(−2)
9		106 867.5(−1)	106 859.10(+10)
10		106 884.7(−4)	106 876.45(+1)
11		106 904.6(+1)	106 895.83(+19)
12		106 924.7(−9)	106 915.23(−134)[a]
13		106 948.1(−3)	106 939.27(+1)
14			106 963.85(+17)
15		107 000.4(+10)	106 989.59(−27)
T	109 437.7(9)	106 788.47(23)[b]	106 780.48(6)[c]
B	0.854(42)	0.8788(21)[b]	0.8724(3)[c]
r(Å)	1.70	1.635	1.6382
σ_{fit}	1.6	0.55[b]	0.14[c]

[a]Perturbed level, not included in the least-squares fit.
[b]Line measurements of Casey (Ref. 9) reduce to 106 788.57(18) and 0.8782(15), with $\sigma_{fit}=0.43$.
[c]Preliminary data reported by Eidelsberg *et al.* (Ref. 43), extended to $J'=14$ and corrected [Ref. 11] by +0.9 cm^{-1}, reduce to 106 780.28(7) and 0.8728(7), with $\sigma_{fit}=0.16$.

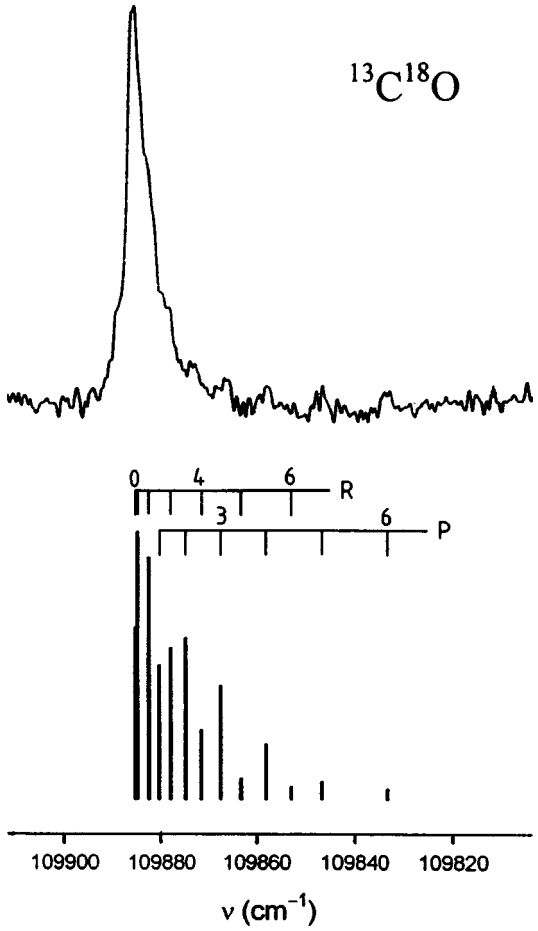

FIG. 9. The $C'\leftarrow X$ 11–0 band of $^{13}C^{18}O$. The stick spectrum has been calculated with $\nu_0=109\,884$ and $B=0.754\ \mathrm{cm}^{-1}$ for a rotational temperature of 20 K.

but one of the diffuse C' levels in Table V can be observed from $v=0$ of the ground state. They must be capable of reaching into the Franck-Condon allowed region, probably through interactions with high vibrational levels of mixed $B\sim D'$ character. For the time being, the limited range of the observations, the weakness of the bands, and the diffuseness of the upper-state levels prevent a more detailed investigation of this complex region of the CO spectrum.

C. Perturbations of the low-*n p* complexes

1. $X^+(0)4p$, $X^+(1)3d\pi$ (102 950–103 400 cm^{-1})

A detailed description of the spectrum in the region of the $X^+(0)4p$ complex may be found in Ref. 25, including a reproduction of the jet absorption spectra of three isotopomers together with their tentative interpretation in terms of one p complex interacting with two $^1\Pi$ non-Rydberg levels. Least-squares calculations based on this model produce unsatisfactory results. More successful is a model which, in addition to $X^+(0)4p$, includes the π component of the $X^+(1)3d$ complex, both interacting with a single $^1\Pi$ perturber. For $^{13}C^{16}O$, $^{12}C^{18}O$, and $^{13}C^{18}O$, the line wave numbers used by the least-squares calculations, together with the differences obs-calc, have been listed in Tables A-II–A-IV of the Appendix.[36] For convenience, Table VI provides a summary of the input data used by the fits, including a description of the experiments and, where necessary, short comments regarding small modifications of the published data. It also includes references for $^{12}C^{16}O$ where the observations remain incomplete and the least-squares fits unsuccessful.

Table VII and Figure 10 show the results of the least-squares fits. Their primary goal is the characterization of the $^1\Pi$ perturber whose identification with $E(v=6)$ will be explained below. Wherever possible, the parameters of the Rydberg levels are kept fixed at the values for the respective ion cores, and Rydberg–Rydberg interactions with $\Delta v\neq 0$ are assumed to be zero. The $E(6)$ perturber is seen to scan rapidly through the region occupied by the Rydberg levels, crossing $X^+(0)4p\pi$ and $X^+(1)3d\pi$ of the intermediate isotopomers before diving into $X^+(0)4p\sigma$ of $^{13}C^{18}O$.

The emerging $4p\pi(0)$ level is virtually unaffected by isotopic substitution, and as anticipated for a Rydberg level built on $v=1$ of the $^2\Sigma^+$ ion core, $3d\pi(1)$ moves from $\sim$25 cm^{-1} above $4p\pi(0)$ of the intermediate isotopomers to $\sim$31 cm^{-1} below $4p\pi(0)$ in $^{13}C^{18}O$. Unexplained is the anomalously large centrifugal distortion of $3d\pi(1)$ for $^{13}C^{16}O$ and $^{12}C^{18}O$, as well as its negative sign in $^{13}C^{18}O$. The $3d\pi(1)$ level forms part of a d complex that also includes $3d\sigma(1)$, established for $^{12}C^{16}O$ at 101 773 cm^{-1},[3,9] and $3d\delta(1)$ which is dipole forbidden from the ground state. The large separation by $\sim$1550 cm^{-1} of the $d\pi$ from the $d\sigma$ compo-

TABLE V. The $C'\,^1\Sigma^+\leftarrow X\,^1\Sigma^+$ bands assigned in the spectra of four CO isotopomers, and estimated upper-state vibrational constants. Except for the underlined band origins, the wave numbers refer to *R* heads, which practically coincide with the origins of the strongly red shaded bands. Isotope shifts, relative to $^{12}C^{16}O$, and vibrational intervals are shown in italics. The upper-state vibrational constants derive from a mass-reduced plot of the vibronic energies T_{ve} versus $\rho(v+\frac{1}{2})$ with $x=7$. All table entries are in cm^{-1}. The residuals o-c are rounded off to the nearest cm^{-1}.

ν	12–16	o−c		13–16	o−c		12–18	o−c		13–18	o−c
$x+4$	110 314	+6	*−214*	110 099.74	−8	*−224*	110 089.85	−1	*−428*	109 885.88	0
	876										
$x+3$	109 437.7	+2		*1 679.98*			*1 681.17*			*1 622.75*	
	862.5										
$x+2$	108 575.2	−3	*−155.4*	108 419.76	−3	*−166.5*	108 408.68	−1	*−312.1*	108 263.13	+13
	1 689			*1 631.29*			*1 628.20*			*1 582*	
x	106 886	−18	*−98*	106 788.47	−2	*−106*	106 780.48	−1	*−205*	106 681	+15

$C'\,^1\Sigma^+$: $T_e=102\,207(118)$; $\omega_e=718(26)$; $\omega_e x_e=-7.0(14)$.

TABLE VI. References to experimental data used by the least-squares analyses of $X^+(0)4p\sigma$, $^1\Sigma^+$ and three strongly mixed $^1\Pi$ levels of four CO isotopomers.

Isotope	State	ν(cm^{-1})	Ref.	Comments
12–16	$X^+(0)4p\sigma$	103 055	44	[a]
			This work	[b]
	$1\,^1\Pi$	103 211	45	[c,d]
			46	[e,d]
			This work	[b]
	$2\,^1\Pi$	103 272	31, 47, 48	[a]
13–16	$X^+(0)4p\sigma$	103 055	31	[a]
	$1\,^1\Pi$	103 161	9	[f,g]
			31	[a]
	$2\,^1\Pi$	103 249	31, 48	[a]
	$3\,^1\Pi$	103 367	9	[f,h]
			This work	[b]
12–18	$X^+(0)4p\sigma$	103 054	This work	[b]
	$1\,^1\Pi$	103 156	This work	[b]
	$2\,^1\Pi$	103 247	This work	[b]
	$3\,^1\Pi$	103 356	This work	[b]
13–18	$X^+(0)4p\sigma$	103 054	49	[a]
	$1\,^1\Pi$	103 078	49	[a]
			This work	[b]
	$2\,^1\Pi$	103 203	31	[a,i]
			This work	[b]
	$3\,^1\Pi$	103 262	31, 48	[a]
			This work	[b]

[a]1VUV+1UV resonance enhanced two photon ionization.
[b]Absorption in a supersonic free jet expansion.
[c]Optogalvanic spectra from $B\,^1\Sigma^+$.
[d]Combined with $B-X$ data of Ref. 40.
[e]2+1 double resonance spectroscopy via $B\,^1\Sigma^+$.
[f]Absorption under equilibrium conditions at room and liquid nitrogen temperatures.
[g]Wave numbers increased by 0.4 cm^{-1}; minor modifications of P and Q line assignments.
[h]J numbering of Q branch increased by 1.
[i]J numbering of Q branch reduced by 2.

nent results partly from $s\sim d$ mixing[13] with $4s\sigma(1)$ at 103 692 cm^{-1}, which lowers the energy of $3d\sigma(1)$, and partly from the interaction with the $\ldots 1\pi^4 5\sigma 2\pi$, $A\,^1\Pi$ precursor, which lifts the $3d\pi(1)$ component into the region of the $X^+(0)4p$ complex and, possibly, of $3d\delta(1)$. It is, thus, conceivable that the anomalous D values of $3d\pi(1)$ reflect the effects of rotational interactions within the d complex that have been neglected by the deperturbation analysis. Also, Cacciani *et al.*[48] observe that with increasing rotation, Q branch transitions to $2\,^1\Pi$ of $^{13}C^{16}O$ and $3\,^1\Pi$ of $^{13}C^{18}O$ show signs of small perturbations that lead for $^{13}C^{18}O$ to the formation of an extra Q head. These recent measurements have not been fitted, but are compared in the appended Tables[36] A-II and A-IV with the lines calculated from the parameters of Table VII.

With an estimated term value of $\sim$103 440 cm^{-1} for $^{12}C^{16}O$, the perturber identified as $E(6)$ fits into a somewhat irregular and very rapidly converging progression of seven $^1\Pi\leftarrow X\,^1\Sigma^+$ bands reported by Ogawa and Ogawa[3] who assigned the first three transitions at 92 930, 95 084, and 97 153 cm^{-1} to $v=0$, 1, and 2 of the $E\,^1\Pi$ state. The reassignment by Eidelsberg and Rostas[11] of the bands at 98 919, 100 651, 102 311, and 104 120 cm^{-1} to a $^3\Pi_1$, rather than $^1\Pi$, upper state turned out to be unfounded when the state specific laser-reduced fluorescence technique of Drabbels *et al.*[46] failed to detect any spin structure and instead revealed a weak rotational interaction of the level at 102 311 cm^{-1} with $v=5$ of $3p\sigma$, $C\,^1\Sigma^+$ at 102 328 cm^{-1}. This perturbation, which is not feasible between $^3\Pi_1$ and $^1\Sigma_0$ states, reveals the partial $3p\pi(v=5)$ character of the $^1\Pi$ level. Figure 11 illustrates the progression with a mass reduced plot of the band origins for four isotopomers,[3,9,11] all increased by the zero-point energies of the neutral ground states and reduced

TABLE VII. Vibronic energies, rotational constants, and interaction energies (in cm^{-1}) for $X^+(0)4p$, $X^+(1)3d\pi$, and $E(6)$ of the 13–16, 12–18, and 13–18 isotopomers of CO. Parameters derived from the incompletely observed $^{12}C^{16}O$ spectra represent effective values. Adjusted parameters are given with 1σ error limits (in parentheses) in units of the last-quoted decimal place. Other parameters are fixed at their estimated values.

		12–16			13–16	12–18	13–18
$X^+(0)4p\sigma$	T_0	103 054.82(3)	$X^+(0)4p\sigma$	T_0	103 054.58(4)	103 054.35(10)	103 054.00(24)
	B_0	1.9675(7)		B_0	1.8809	1.8738	1.8034(7)
	$D_0\times10^5$	1.03(10)		$D_0\times10^5$	4.8(4)	7.0(14)	2.49(7)
$1\,^1\Pi$	T	103 213.62(4)	$X^+(0)4p\pi$	T_0	103 239.4(11)	103 235.0(22)	103 234.8(5)
	B	1.7526(7)		B_0	1.8809	1.8738	1.7719(7)
	$D\times10^5$	0.81(16)		$D_0\times10^5$	0.56	0.56	0.51
$2\,^1\Pi$	T	103 273.76(4)	$X^+(1)3d\pi$	T_1	103 261.0(14)	103 263.7(42)	103 202.9(8)
	B	1.9596(5)		B_1	1.8631	1.8561	1.6842(17)
	$D\times10^5$	0.55(13)		$D_1\times10^5$	15.9(7)	23.7(34)	−5.5(10)
			$E(6)$	T_6	103 282.7(5)	103 265.6(37)	103 107.9(4)
				B_6	1.3837(17)	1.412(15)	1.4161(24)
				$D_6\times10^5$	5.2	5.2	
$\langle 1\,^1\Pi\|H_r\|4p\sigma(0)\rangle$		2.28[a,b]	$\langle 4p\sigma(0)\|H_r\|4p\pi(0)\rangle$		3.030(20)[a]	2.94(5)[a]	3.030[a]
$\langle 2\,^1\Pi\|H_r\|4p\sigma(0)\rangle$		2.148(29)[a]	$\langle 4p\pi(0)\|H_{ev}\|E(6)\rangle$		72.5(8)	67.4(34)	66.4(6)
			$\langle 3d\pi(1)\|H_{ev}\|E(6)\rangle$		70.7(8)	72.5(31)	−21.1(23)
	$\sigma_{\rm fit}$	0.13		$\sigma_{\rm fit}$	0.16	0.29	0.13

[a]J-independent electronic factor α of the matrix element [Eq. (3)].
[b]Value estimated from the data of Drabbels *et al.* (Ref. 46).

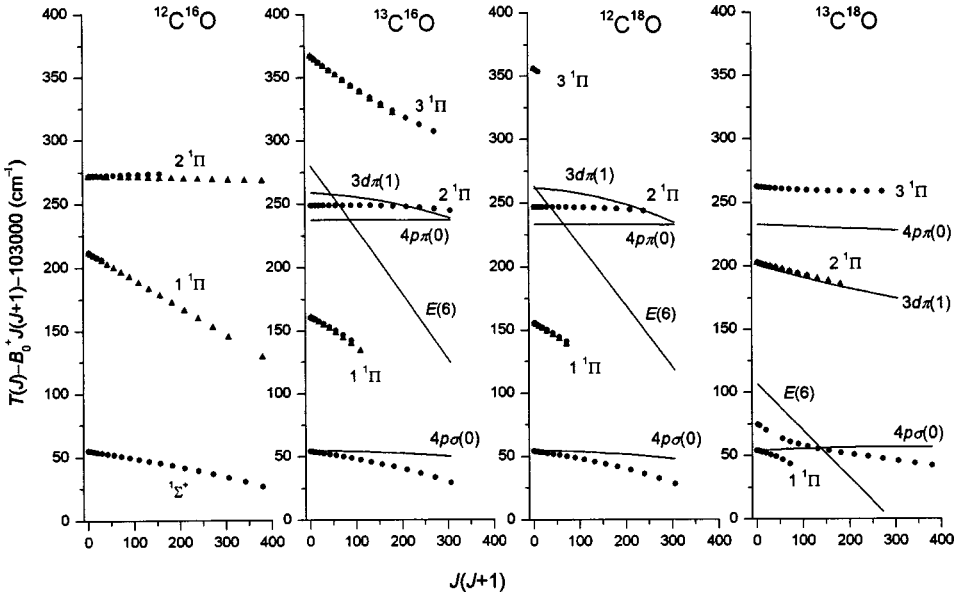

FIG. 10. The $4p(0)$ complex and $3d\pi(1)$ of four CO isotopomers in interaction with $E(6)$. Full circles and triangles represent reduced term values for the observed *e* and *f* parity levels, respectively, solid lines refer to the deperturbed terms. Observations for the main isotope are incomplete and have not been deperturbed.

by the vibrational energies of the ion cores. The steeply descending E state curve reflects the decreasing vibrational intervals of the progression and is in line with *ab initio* calculations[15] that predict a rapid change from $\ldots 1\pi^4 5\sigma 3p\pi$ Rydberg to $\ldots 1\pi^3 5\sigma 2\pi^2$ valence state character. Significant downward shifts of the $v=3$ and 4 levels may indicate additional interactions with the core excited $\ldots 1\pi^3 5\sigma^2 3s\sigma$, $^1\Pi$ state which appears in the absorption spectrum with a perturbed vibrational progression extending from 102 807 cm^{-1} to higher energies.

The failure to deperturb the spectrum of $^{12}C^{16}O$ is undoubtedly linked to the lack of observations on the third $^1\Pi$ state arising from the interaction of $E(6)$ with $4p\pi(0)$ and $3d\pi(1)$. Nevertheless, the effective rotational interaction matrix elements with $4p\sigma(0)$ (Table VII) show the two observed $^1\Pi$ levels to be mixed with approximately equal percentages of $4p\pi(0)$ character.

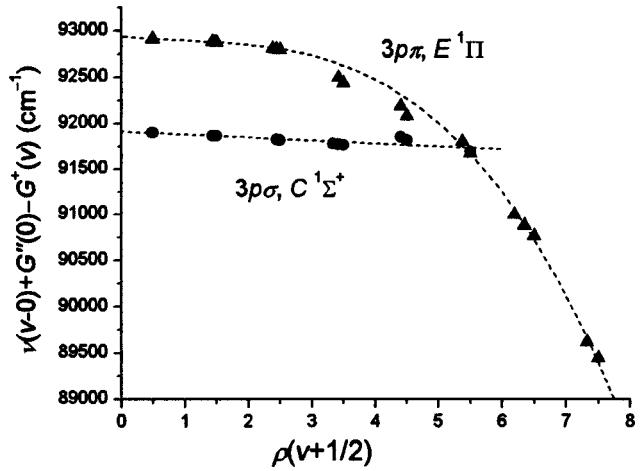

FIG. 11. Mass reduced plots of the reduced vibronic terms for the $3p\sigma$ and $3p\pi$ Rydberg states of four isotopomers; ρ^2 is the ratio of the reduced masses, μ/μ_i. $G^+(v)$ is the vibrational energy of the ion core.

2. $X^+(2)4p$, $X^+(0)5p$ (106 900–107 600 cm^{-1})

Figure 12 shows the jet absorption spectra of four CO isotopomers recorded at the Meudon 10-m spectrograph. At the longest wavelengths, the weak diffuse feature labeled *a* represents the $C'\ ^1\Sigma^+(v=7)$ valence state level already discussed in Sec. III B. In all four spectra, the 0–0 transition to the Σ component of $X^+(0)5p$, *c*, is clearly recognizable from its conspicuous zero gap at 107 174 cm^{-1} and from its nearly undergraded structure for low rotation. Except for the very weak feature labeled *e*, all other bands represent $^1\Pi \leftarrow {}^1\Sigma$ transitions. For $^{12}C^{16}O$, they include the narrow continuum *b* at 107 160 cm^{-1} whose upper state, a loosely bound and strongly predissociated level, extensively mixes with the nearest $^1\Pi$ states of higher energies. The bands at 107 335 and 107 410 cm^{-1} of the main isotope, *d* and *f*, reflect the effects of these interactions with strongly red shaded *R*, *Q*, and *P* branches of broad and only partly resolved lines. The more distant bands at 107 520 and 107 682 cm^{-1}, *g* and *h*, consist of sharper lines and gradually resume the undergraded structure typical of transitions to unperturbed Rydberg levels built on the ground state of CO^+. The final state of band *h*, probably $X^+(3)3d\pi$, seems only marginally involved with the lower levels and is not included in the least-squares calculation. An expanded view of the spectrum from 107 100 to 107 450 cm^{-1}, complete with rotational assignments, can be found in Fig. 5 of Ref. 50. Note, however, that for band *d* at 107 335 cm^{-1} the $P(11)$ and $Q(13)$ identifications must be reversed.

Eikema *et al.*[31] report the very weak and narrow lines of an additional Σ–Σ band of $^{12}C^{16}O$ at 107 366 cm^{-1} of the two-photon ionization spectrum (see Fig. 7 of Ref. 31). The quantum defect points to a $4p\sigma$ upper state with $v=2$ which makes this level Franck–Condon forbidden from $v=0$ of the ground state and the transition too weak to be seen in the absorption spectrum. However, on account of an avoided crossing with the *e* parity levels of the broadened $^1\Pi$ state at 107 410 cm^{-1}, the *R* branch converges near 107 395 cm^{-1},

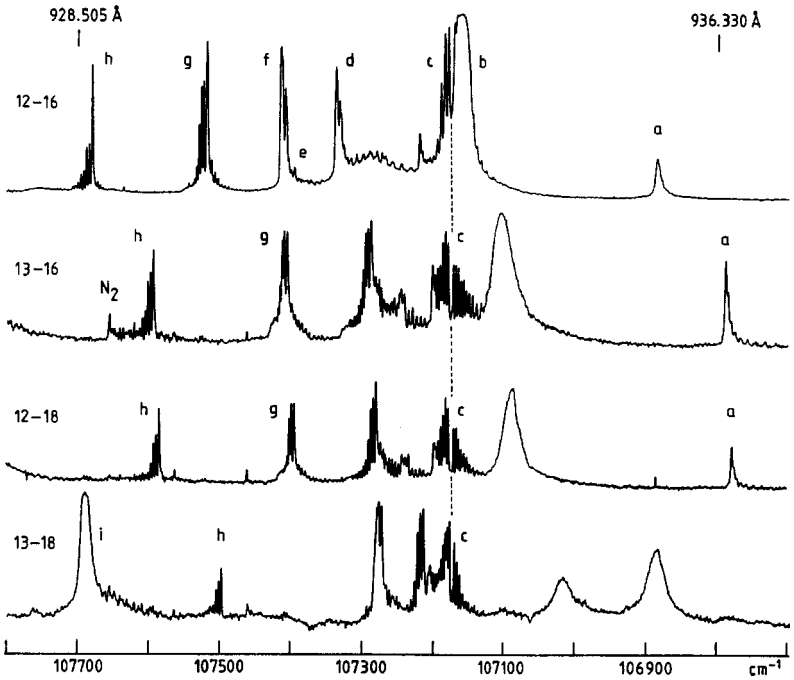

FIG. 12. Jet absorption spectra of four CO isotopomers in the 106 700–107 800 cm^{-1} region. The upper states of the transitions are (a) $C'\,{}^1\Sigma^+(v=7)$; (b) $1\,{}^1\Pi$; (c) $X^+(0)5p\sigma$, (d) $2\,{}^1\Pi$; (e) $X^+(2)4p\sigma$; (f) $3\,{}^1\Pi$; (g) $X^+(2)4p\pi$; (h) $X^+(3)3d\pi$; (i) $A^+(3)3s\sigma$.

and it is this accumulation of lines which contributes to the weak feature *e* of the $^{12}C^{16}O$ absorption spectrum in Fig. 12.

There is no direct evidence for the $^1\Pi$ upper-state symmetry of the diffuse band *b* at 107 160 cm^{-1}. Under conditions that lead to complete saturation in the region of peak absorption, a very diffuse and strongly red-shaded *R* and the accompanying *P* branch are found to emerge from its longward wing; *Q* lines and the head forming *R* lines remain confined to the region of total absorption. However, for low rotation, as pointed out previously,[50] the diffuse state reveals its partial $5p\pi$ character through rotational mixing with the $5p\sigma$ levels. This is particularly evident from the 1 VUV +1 UV photoionization spectra of Fig. 13 where transitions to $5p\sigma(0)$ levels other than $J'=0$ are either absent or very weak and broad on account of the shortened lifetimes of the levels reached by the VUV photons. $J'=0$ remains pure Σ. The different widths and intensities of the $P(1)$ lines in the 12–16 and 13–16 spectra, both recorded simultaneously and in natural abundance, point to an additional dissociative decay channel that reduces the upper-state lifetimes of at least $^{12}C^{16}O$. The deperturbation analysis shows the $X^+(0)5p\pi$ Rydberg level to be dispersed over at least two states. With increasing *J*, its interaction with $5p\sigma(0)$ shifts from the diffuse $^1\Pi$ upper state of band *b* to that of band *d*, leading to the formation of conspicuous *R* heads in transitions to $5p\sigma(0)$ of the 12–16, 13–16, and 12–18 isotopomers.

The present analysis is restricted to the spectrum of $^{12}C^{16}O$. Most of the experimental data used by the least-squares fits come from jet absorption spectra photographed at the Photon Factory synchrotron facility. Data relating to $X^+(2)4p\sigma$ are from Table 7 of Ref. 31. The very faint and broad *R* and *P* lines of the diffuse transition at 107 160 cm^{-1}, observed for $J=9-13$ and 5–14, respectively, had to be interpolated on photographically enlarged room temperature spectra from the Meudon laboratory. Accordingly, their accuracy is limited, and the same can be said of wave numbers derived from the broad and only partially resolved lines in the 107 335 and 107 410 cm^{-1} bands. The poor precision affects the performance of the least-squares fits, and in order to assure proper convergence of the calculations, it was important to keep the number of adjustable parameters as small as possible. Table A-V[36] collects the experimental data, together with the residuals obs−calc. Table VIII and Fig. 14 summarize the final results of the data reduction.

The deperturbed structures emerging from the least-squares calculations are unambiguously those of two *p* complexes crossed by two Π levels of much smaller rotational constants. The Σ and Π components of $4p(2)$ and $5p(0)$ are separated by 148 and 116 cm^{-1}, respectively, in rough qualitative agreement with expectations based on the ~180 cm^{-1} separation established for $4p(0)$ and the assumption that

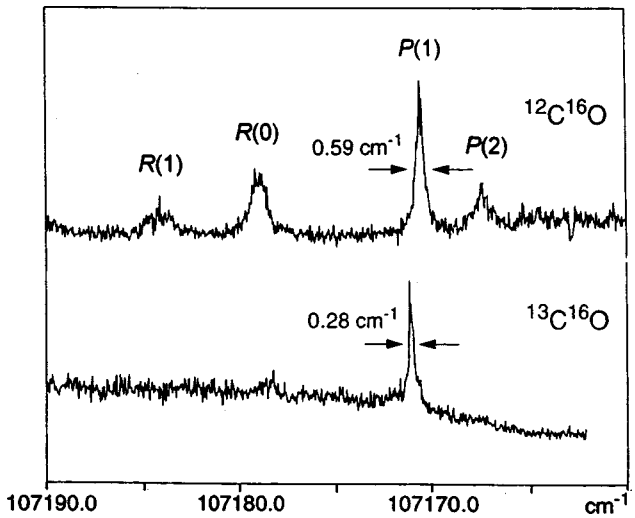

FIG. 13. Two-photon ionization spectra of the low-*J* lines in the $X^+(0)5p\sigma\leftarrow X(0)$ bands of $^{12}C^{16}O$ and $^{13}C^{16}O$, both recorded simultaneously and in natural abundance.

TABLE VIII. Vibronic energies, rotational constants, and interaction energies (cm^{-1}) for the deperturbed $X^+(0)5p$ and $X^+(2)4p$ complexes and two $^1\Pi$ perturbers of $^{12}C^{16}O$. Adjusted parameters are given with 1σ error limits (in parentheses) in units of the last-quoted decimal place. Other parameters are fixed at their estimated values.

	T_v	B_v	$D_v\times10^5$	Interactions	
$X^+(0)5p\sigma$	107 174.10	2.1227(49)	51.0(61)	$\langle 5p\sigma(0)\|H_r\|5p\pi(0)\rangle$	3.50(22)[a]
$I\,^1\Pi$	107 256.4(10)	0.5000(63)	1.00	$\langle 5p\sigma(0)\|H_r\|II\,^1\Pi\rangle$	−1.31(17)[b]
$X^+(0)5p\pi$	107 290.4(18)	1.893(10)	0.63	$\langle 5p\pi(0)\|H_{ev}\|I\,^1\Pi\rangle$	111.93(80)
$II\,^1\Pi$	107 359.9(22)	1.3517(91)	0.63	$\langle 5p\pi(0)\|H_{ev}\|II\,^1\Pi\rangle$	48.91(79)
$X^+(2)4p\sigma$	107 365.90	1.92935	0.63	$\langle 4p\sigma(2)\|H_r\|4p\pi(2)\rangle$	2.222(48)[a]
$X^+(2)4p\pi$	107 514.3(14)	1.8184(49)	0.63	$\langle 4p\sigma(2)\|H_r\|II\,^1\Pi\rangle$	−1.04(15)[b]
				$\langle 4p\pi(2)\|H_{ev}\|I\,^1\Pi\rangle$	37.0(41)
				$\langle 4p\pi(2)\|H_{ev}\|II\,^1\Pi\rangle$	7.0(37)
		σ_{fit}	0.40		

[a]J-independent electronic factor α of the matrix element [Eq. (3)].
[b]J-independent factor of the matrix element. The heterogeneous interaction is arbitrarily assumed to be of the form given by Eq. (3).

$\Delta\nu(\Pi,\Sigma)$ scales according to ν^{-3}, ν being the effective principal quantum number.

The rotational constant of $5p\sigma(0)$ is larger than expected and is accompanied by an unduly large D value. Together, they compensate for the apparent inability of the calculations to fully reproduce the rotational interaction of $5p\sigma(0)$ with the fraction of $5p\pi(0)$ mixed into the $I\,^1\Pi$ perturber of lower energy. Also, it is hard to understand how the latter, having a B value of 0.500 cm^{-1} and an internuclear distance of 2.22 Å, is capable of perturbing a Rydberg level of only half this r value with an interaction matrix element as big as 112 cm^{-1}. Probably, the perturber is of mixed character facilitating its overlap with the Rydberg level. An admixture of the core excited $A^+3s\sigma$ configuration is one possibility suggested by the *ab initio* calculations of Cooper and Kirby.[15]

The $II\,^1\Pi$ perturber with a B value of 1.352 cm^{-1} resembles the highest observed E state vibronic levels, including the $E(6)$ perturber of $4p\pi(0)$ and $3d\pi(1)$. However, at an energy of 3240 cm^{-1} above $E(7)$, and considering the irregular nature of the E state progression, the $II\,^1\Pi$ level is too far removed for the connection with $E\,^1\Pi$ to be made with confidence. The perturber mixes rotationally with $4p\sigma(2)$ and $5p\sigma(0)$. The two interaction matrix elements are small, of the order of 1 cm^{-1}, but their inclusion in the least-squares calculations does improve the overall quality of the fit.

3. $X^+(4)4s, X^+(3)4p, X^+(1)5p$ (109 300–109 650 cm^{-1})

The absorption spectrum in the 91.23–91.49 nm region of $^{12}C^{16}O$ has previously been described by Rostas *et al.*[25] and Huber.[50] The latter includes a figure that illustrates the strongly isotope dependent predissociation which transforms the comparatively sharp structure at around 109 450 cm^{-1} of the main isotope into diffuse, structureless bands near 109 320 cm^{-1} of $^{13}C^{16}O$ and $^{12}C^{18}O$ and overlapping, in $^{13}C^{18}O$, the $6p(0)$ complex at ~109 180 cm^{-1}. The band assignments proposed in Refs. 25 and 50 derive from detailed fine structure analyses and are supported by ion-dip spectra observed from $v=1$ of the $3s\sigma, B\,^1\Sigma^+$ state (see Figs. 2 and 3 of Ref. 13). The present work adds the deperturbation of the spectra based on high resolution absorption data obtained at the Photon Factory synchrotron facility in Tsukuba and reproduced in Figs. 15(a) and 15(b), as well as on two-photon ionization spectra recorded at the Laser Center of the Vrije Universiteit in Amsterdam and displayed by Figs. 15(c)–15(e). The line wave numbers, together with the residuals obs−calc, can be found in the appended Table A-VI.[36] For $X^+(1)5p\sigma$, which appears neither in the ab-

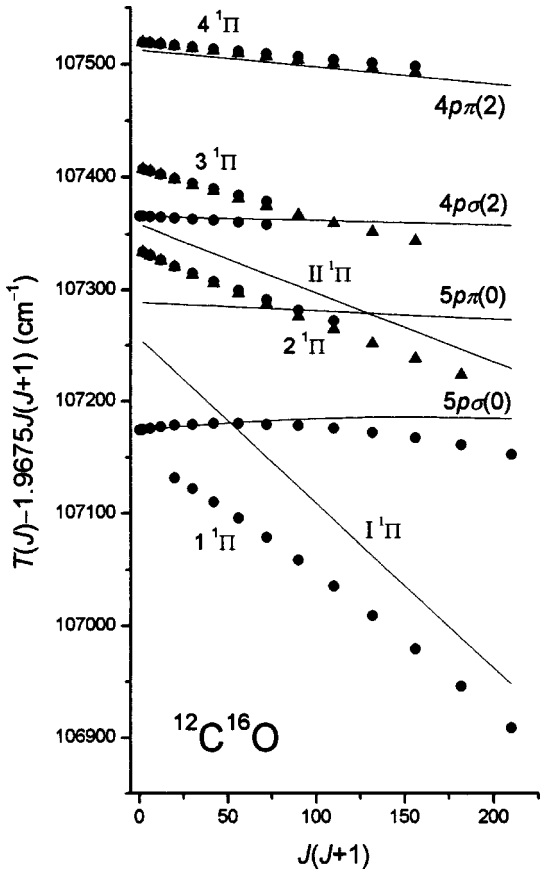

FIG. 14. Reduced term values for the $4p(2)$ and $5p(0)$ complexes and two $^1\Pi$ perturbers of $^{12}C^{16}O$. Full circles and triangles refer to the observed e and f parity levels, respectively, deperturbed terms are shown by solid lines.

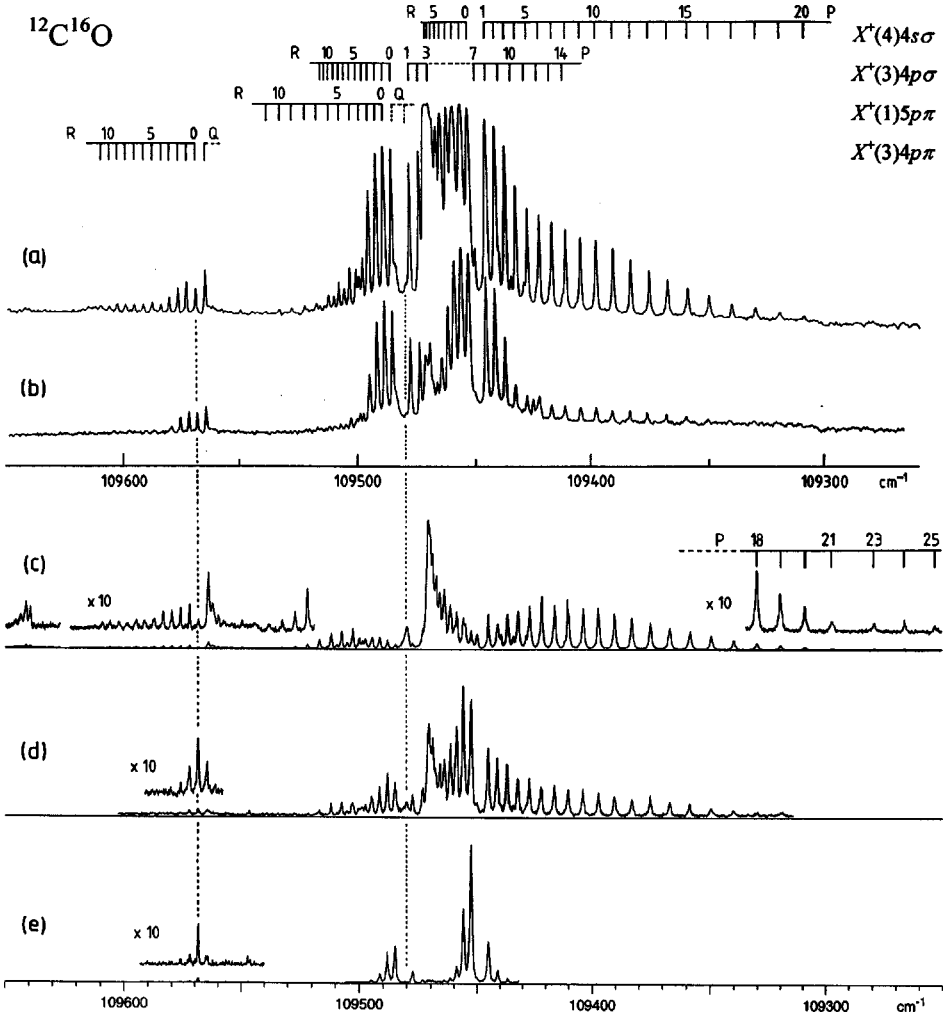

FIG. 15. (a) and (b) Jet absorption and (c)–(e) two-photon ionization spectra of $^{12}C^{16}O$ in the 109 250–109 650 cm^{-1} region, the latter recorded for three widely different rotational temperatures.

sorption nor in the photoionization spectra, the term values come from Table II of Ref. 13. Table IX reports the final parameters, and Fig. 16 compares the deperturbed with the observed perturbed Rydberg complexes.

From the B value in Table IX, the internuclear separation in the level tentatively assigned as $X^+(4)4s\sigma$ is found to be 1.19 Å, close to the internuclear distance at the crossing of the diabatic $4s\sigma$ Rydberg and $D'\,^1\Sigma^+$ valence state potentials of Fig. 1. In reality, the crossing is avoided, and the transition to the mixed $4s\sigma(4)$ level is analogous to the resonances arising at lower energies from the similarly mixed $3s\sigma$, $B\sim D'$ levels discussed in Sec. III A.

The $X^+(3)4p\sigma$ level, Franck-Condon forbidden from $v=0$ of the ground state, gains its intensity through homogeneous interaction with $4s\sigma(4)$, and a similar transfer of intensity appears to benefit the e parity levels of $X^+(1)5p\pi$ which acquire, with increasing rotation, growing amounts of $X^+(1)5p\sigma$ character. The $5p\sigma$ level is not seen in absorp-

TABLE IX. Vibronic energies, rotational constants, and interaction energies (cm^{-1}) for the deperturbed $X^+(4)4s$, $X^+(3)4p$, and $X^+(1)5p$ complexes and one $^1\Pi$ perturber of $^{12}C^{16}O$. Adjusted parameters are given with 1σ error limits (in parentheses) in units of the last-quoted decimal place; others are fixed at their estimated values.

State	T	B	$D\times10^5$	Interactions	
$X^+(1)5p\sigma$[a]	109 353.00	1.948 43	0.63	$\langle X^+(1)5p\sigma\|H_r\|X^+(1)5p\pi\rangle$	3.517(72)[b]
$X^+(4)4s\sigma$	109 460.63(49)	1.736 95(98)	0.70(46)	$\langle X^+(4)4s\sigma\|H_{ev}X^+(3)4p\sigma\rangle$	15.487(39)
$X^+(3)4p\sigma$	109 469.60(97)	1.910 23	0.63	$\langle X^+(4)4s\sigma\|H_r\|^1\Pi\rangle$	0.149(34)[c]
$X^+(1)5p\pi$	109 479.9(28)	1.9202(57)	0.63	$\langle X^+(3)4p\sigma\|H_r\|X^+(3)4p\pi\rangle$	2.04(10)[b]
$^1\Pi$	109 483.8(21)	1.6911(18)	1.00	$\langle X^+(1)5p\pi\|H_{ev}\|^1\Pi\rangle$	4.44(49)
$X^+(3)4p\pi$	109 566.57(12)	1.8722(26)	0.63		
		σ_{fit}	0.14		

[a]The observed term values are taken from Komatsu *et al.* (Ref. 13).
[b]J-independent electronic factor α of the matrix element [Eq. (3)].
[c]J-independent factor of the matrix element, assuming the heterogeneous interaction to be of the form given by Eq. (3).

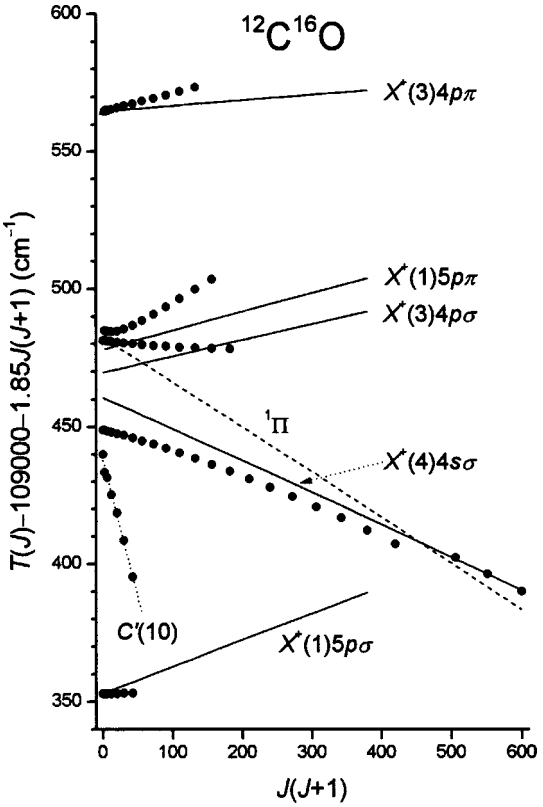

FIG. 16. Reduced term values for the $4s(4)$, $4p(3)$, and $5p(1)$ complexes of $^{12}C^{16}O$. Full circles and triangles refer to the observed *e* and *f* parity levels, solid lines to deperturbed terms. The dashed line represents a $^1\Pi$ level assumed to be responsible for perturbations of the low-*J* levels in $5p\pi(1)$ and small irregularities near $J=21$ of $4s\sigma(4)$. Data for $X^+(1)5p\sigma$ are taken from Ref. 13. For a discussion of $C'(10)$ see Sec. III B above.

tion. It appears prominently in the ion-dip spectra from $v=1$ of $3s\sigma,B\,^1\Sigma^+$,[13] but the very limited range and low precision of the data prevent us from including the $4s\sigma(4)\sim 5p\sigma(1)$ interaction in the least-squares calculations. The *f* parity levels for $J=1-5$ of $5p\pi(1)$ have also been observed from $B(v=1)$.[13] For low rotation, both parities are perturbed by a dark $^1\Pi$ level of smaller *B* value. On the assumption that the same perturber is responsible for small irregularities near $P(22)$ of the $X^+(4)4s\sigma$ band [see Figs. 15(c) and 16], its rotational constant can be estimated at 1.691 cm^{-1}.

At the rotational temperatures of the spectra, most of the *Q* lines of the $5p\pi(1)$ band are calculated to fall into the zero gap of $4p\sigma(3)$ where a number of diffuse and strongly temperature dependent features appear in the spectra of Fig. 15. In the absorption spectra of traces (a) and (b), a shoulder at 109 483.5 cm^{-1}, just longward of the $R(0)$ line associated with $4p\sigma(3)$, represents the unresolved *Q* branch from $J=1$ to 4, and a much weaker shoulder at 109 479.4 cm^{-1}, shortward of $P(1)$, marks the location where the initially red shaded *Q* branch begins to converge again. The two-photon ionization spectra of traces (c)–(e) are quite different. Even at the lowest temperature, the low-*J Q* lines seem to be absent, and with increasing temperature, the shoulder at 109 479 cm^{-1} develops into a head-like feature degraded to shorter wavelengths. Very likely, the absence from the photoionization spectra of low-*J Q* lines in the $5p\pi(1)$ band and of $P(22)$ in $4s\sigma(4)$ points to predissociation of the upper-state levels induced by the $^1\Pi$ perturber. In contrast, transitions to unperturbed *f* parity levels of higher *J*, barely seen in absorption, clearly benefit from the greater sensitivity of the photoionization spectra.

For $J>10$, the *e* parity levels of $X^+(3)4p\pi$ at 109 567 cm^{-1} show signs of an interaction with an unknown state of higher energy. Casey[9] already noticed additional structure at 109 640 cm^{-1} in the absorption spectrum of $^{12}C^{16}O$, and the same lines appear in the two-photon ionization spectrum of Fig. 15(c). From the available data we are unable to establish their connection, if any, with $v=3$ of the $4p$ complex.

IV. CONCLUSIONS

The work reported in the preceding sections forms part of a systematic review of the absorption spectra of CO in the 90–100 nm region. Aided by upper-state identifications made by Ebata *et al.* from triple-resonant photoionization[4,12] and ion-dip[7,13] spectra, we conclude that most of the bands arise from transitions to *s,p,d*, but not *f*, complexes built on $X\,^2\Sigma^+$ of CO^+. The Rydberg levels are subject to homogeneous interactions with several perturber states, foremost among them the mostly repulsive $D'\,^1\Sigma^+$ valence state[14,16–19] which holds the key to the diffuseness of many members of the $^1\Sigma^+$ Rydberg series. The avoided crossing of $3s\sigma,B\,^1\Sigma^+$ with the D' state[17,18] precedes a similar interaction of the *B* state with $C'\,^1\Sigma^+$ at higher energies, allowing the loosely bound C' valence state to reach into the Franck-Condon region and to make some of its vibrational levels accessible from $v=0$ of the neutral ground state.

One of the perturbers involved with the $X^+(v)4p\pi$ and $5p\pi$ Rydberg levels is the $n=3$ lowest member of the $p\pi$ series. Configuration mixing with the $\ldots 1\pi^3 5\sigma 2\pi^2$, $^1\Pi$ valence state[15] facilitates its interactions with the higher members in violation of the $\Delta v=0$ selection rule. A second $^1\Pi$ perturber, with $B=0.500$ cm^{-1} and strongly predissociated, is probably best described by a mixture of $\ldots 1\pi^3 5\sigma 2\pi^2$ and $\ldots 1\pi^3 5\sigma^2 6\sigma$.[15] Largely unexplored is the role played by the core excited $\ldots 1\pi^3 5\sigma^2 3s\sigma$, $^1\Pi$ Rydberg state[15] which overlaps the region of the $X^+(v)4p$ and $5p$ complexes with an irregular progression of red shaded and partly diffuse $^1\Pi\leftarrow{}^1\Sigma^+$ bands.

The Edlén plots of Fig. 17 display the $p\sigma$ and $p\pi$ quantum defects that result from the analyses of the $^{12}C^{16}O$ spectra. The σ levels are seen to present a nearly unperturbed behavior, with only minor irregularities arising in $n=3$ and 4 from interactions with $D'\,^1\Sigma^+$. In contrast, the π quantum defects for $n=3$, rapidly increasing with v, reflect growing admixtures of valence character in the *E* state vibronic levels. The $n=4$ levels are similarly affected, and even for $n=6$ and 7, the quantum defects indicate the $v=0$ levels to deviate from their expected positions by as much as ± 20 cm^{-1}. Although most of the analyses described in the preceding sections reproduce the observed spectra satisfactorily, it is clear that the derived parameters have local significance only, and that eventually a more global approach, similar to the multichannel quantum defect methods applied by Jungen *et al.*[27] to the analysis of the near-threshold spectrum of N_2,

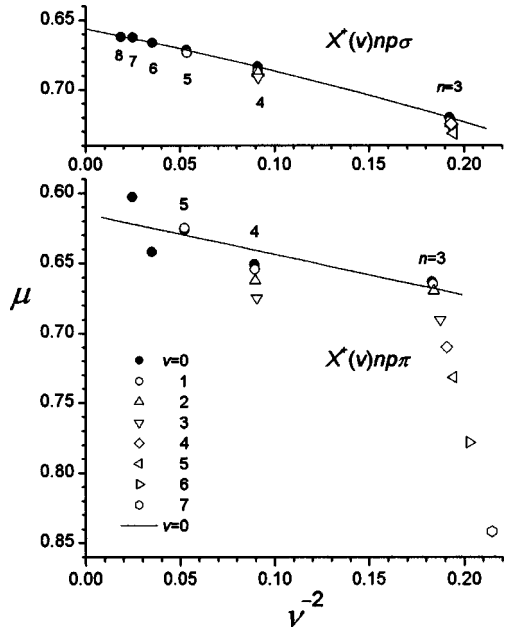

FIG. 17. Edlén plots of the quantum defects μ for the $X^+(v)np\sigma$ and $X^+(v)np\pi$ Rydberg levels of $^{12}C^{16}O$; ν is the effective principal quantum number.

must be taken if a consistent description of the CO rovibronic structures and interactions is to be achieved.

The transition from essentially pure $np\pi$ Rydberg to significant valence state character is further emphasized by the strong v dependence of the rotation independent factor α of the l uncoupling matrix element in Eq. (3) and shown in Fig. 18 for p complexes with $n \leqslant 5$. From $v=0$ to 5, α decreases more or less linearly by a factor of ~ 5. However, already for $v=0$, the observed value of 3.5 cm^{-1} is 11% smaller than calculated for $l=1$. Ebata *et al.*[4,13] report similar results for p complexes ranging from $n=4$ to 9 where the observed l uncoupling for $v=0$ and 1 is best reproduced assuming $l=0.8$, corresponding to a reduction of α by 15%. The consistency of the observations over a wide range of n seems to suggest that for the lowest vibrational quantum numbers the quenching of α is not so much the work of Rydberg–valence interactions, but might be effected by the dipolar ion core. Under these conditions, Watson[51] has shown that the perpendicular components of the orbital angular momentum are quenched by a factor of

$$\{1-\mu^2/[2l^2(l+1)^2]\}, \tag{4}$$

where μ, in atomic units ea_0, represents the core dipole moment taken at the center of mass. With an *ab initio* calculated dipole moment[52] of 2.5 Debye, or 1 ea_0, the l uncoupling matrix element will be reduced by 13%.

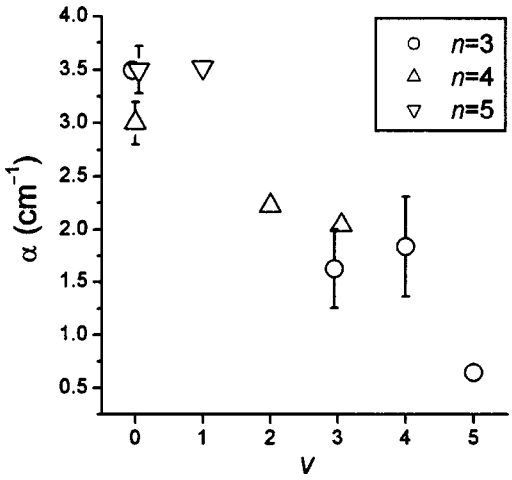

FIG. 18. The rotation independent factor α of the l uncoupling matrix element [Eq. (3)] for np complexes with $n \leqslant 5$, plotted as a function of v. Results for $n=3$ derive from unpublished data (Ref. 11). For $n=4$ and 5, they are taken from Tables VII–IX. Error bars equal to, or smaller than, ± 0.1 cm^{-1} are not shown.

ACKNOWLEDGMENTS

We are much indebted to Maurìce Benharrous for technical assistance provided during the experimental work at the Observatoire de Paris-Meudon, and to Monique Clémino who assisted in the measurements of the photographic plates. We wish to thank François Rostas for his continuing support of this work, and to acknowledge many stimulating discussions with him as well as with Lydia Tchang-Brillet and Paul Julienne. Work at the Photon Factory has been carried out with the approval of the Photon Factory Advisory Committee (proposals #91-149 and 93G-136), and K.P.H. recalls with pleasure the hospitality enjoyed not only at the Photon Factory, but also during repeated visits to the Observatoire de Paris-Meudon and to the Laser Center of the Vrije Universiteit in Amsterdam. Jim Watson, finally, is acknowledged for his critical reading of the manuscript.

[1] C. Letzelter, M. Eidelsberg, F. Rostas, J. Breton, and B. Thieblemont, Chem. Phys. **114**, 273 (1987).
[2] M. Ogawa and S. Ogawa, J. Mol. Spectrosc. **41**, 393 (1972).
[3] S. Ogawa and M. Ogawa, J. Mol. Spectrosc. **49**, 454 (1974).
[4] T. Ebata, N. Hosoi, and M. Ito, J. Chem. Phys. **97**, 3920 (1992).
[5] W. Kong, D. Rodgers, J. W. Hepburn, K. Wang, and V. McKoy, J. Chem. Phys. **99**, 3159 (1993).
[6] P. Erman, A. Karawajczyk, E. Rachlew-Källne, C. Strömholm, J. Larsson, A. Persson, and R. Zerne, Chem. Phys. Lett. **215**, 173 (1993).
[7] M. Komatsu, T. Ebata, T. Maeyama, and N. Mikami, J. Chem. Phys. **103**, 2420 (1995).
[8] A. Mellinger, C. R. Vidal, and Ch. Jungen, J. Chem. Phys. **104**, 8913 (1996).
[9] M. Casey, Ph.D. thesis, University College, Dublin, 1978.
[10] A. E. Douglas and J. G. Potter, Appl. Opt. **1**, 727 (1962).
[11] M. Eidelsberg and F. Rostas, Astron. Astrophys. **235**, 472 (1990); M. Eidelsberg, J. J. Benayoun, Y. Viala, F. Rostas, P. L. Smith, K. Yoshino, G. Stark, and C. A. Shettle, *ibid.* **265**, 839 (1992); F. Launay *et al.*, unpublished data.
[12] N. Hosoi, T. Ebata, and M. Ito, J. Phys. Chem. **95**, 4182 (1991).
[13] M. Komatsu, T. Ebata, and N. Mikami, J. Chem. Phys. **99**, 9350 (1993).
[14] D. L. Cooper and K. Kirby, J. Chem. Phys. **87**, 424 (1987).
[15] D. L. Cooper and K. Kirby, Chem. Phys. Lett. **152**, 393 (1988).
[16] K. Kirby and D. L. Cooper, J. Chem. Phys. **90**, 4895 (1989).
[17] G. L. Wolk and J. W. Rich, J. Chem. Phys. **79**, 12 (1983).
[18] W.-Ü L. Tchang-Brillet, P. S. Julienne, J.-M. Robbe, C. Letzelter, and F. Rostas, J. Chem. Phys. **96**, 6735 (1992).
[19] J. Baker, W.-Ü L. Tchang-Brillet, and P. S. Julienne, J. Chem. Phys. **102**, 3956 (1995).
[20] D. M. Cooper and S. R. Langhoff, J. Chem. Phys. **74**, 1200 (1981).
[21] S. V. O'Neil and H. F. Schaefer III, J. Chem. Phys. **53**, 3994 (1970).
[22] W. Coughran, J. Rose, T.-I. Shibuya, and V. McKoy, J. Chem. Phys. **58**, 2699 (1973).
[23] Y. Li, R. J. Buenker, and G. Hirsch, Theor. Chem. Acc. **100**, 112 (1998).

[24] W. C. Stwalley, W. T. Zemke, and S. C. Yang, J. Phys. Chem. Ref. Data **20**, 153 (1991); **22**, 87 (1993).
[25] F. Rostas, F. Launay, M. Eidelsberg, M. Benharrous, C. Blaess, and K. P. Huber, Can. J. Phys. **72**, 913 (1994).
[26] K. P. Huber and Ch. Jungen, J. Chem. Phys. **92**, 850 (1990).
[27] Ch. Jungen, K. P. Huber, M. Jungen, and G. Stark, J. Chem. Phys. **118**, 4517 (2003).
[28] P. F. Levelt and W. Ubachs, Chem. Phys. **163**, 263 (1992).
[29] K. Ito, T. Namioka, Y. Morioka, T. Sasaki, H. Noda, K. Goto, T. Katayama, and M. Koike, Appl. Opt. **25**, 837 (1986).
[30] K. P. Huber, G. Stark, and K. Ito, J. Chem. Phys. **98**, 4471 (1993).
[31] K. S. E. Eikema, W. Hogervorst, and W. Ubachs, Chem. Phys. **181**, 217 (1994).
[32] W. Ubachs, K. S. E. Eikema, and W. Hogervorst, Appl. Phys. B: Photophys. Laser Chem. **57**, 411 (1993).
[33] S. Gerstenkorn and P. Luc, *Atlas du spectre d'absorption de la molécule de l'iode entre 14 800–20 000* cm^{-1}, *CNRS, Paris (1978); see also Rev. Phys. Appl.* **14**, 791 (1979).
[34] G. Guelachvili, D. de Villeneuve, R. Farrenq, W. Urban, and J. Vergès, J. Mol. Spectrosc. **98**, 64 (1983).
[35] R. Farrenq, G. Guelachvili, A. J. Sauval, N. Grevesse, and C. B. Farmer, J. Mol. Spectrosc. **149**, 375 (1991).
[36] See EPAPS Document No. E-JCPSA6-121-007425 for line wave numbers and term values. A direct link to this document may be found in the online article's HTML reference section. The document may also be reached via the EPAPS homepage (http://www.aip.org/pubservs/epaps.html) or from ftp.aip.org in the directory /epaps/. See the EPAPS homepage for more information.
[37] M. Monnerville and J. M. Robbe, J. Chem. Phys. **101**, 7580 (1994); L. Andric, T. P. Grozdanov, R. McCarroll, and W.-Ü L. Tchang-Brillet, J. Phys. B **32**, 4729 (1999).
[38] O. Atabek and R. Lefebvre, Chem. Phys. Lett. **17**, 167 (1972).
[39] Ch. Jungen, J. Chem. Phys. **53**, 4168 (1970).
[40] M. Eidelsberg, J.-Y. Roncin, A. Le Floch, F. Launay, C. Letzelter, and J. Rostas, J. Mol. Spectrosc. **121**, 309 (1987).
[41] T. Ebata, T. Sutani, and N. Mikami, Chem. Phys. Lett. **240**, 357 (1995).
[42] R. F. Barrow, G. G. Chandler, and C. B. Meyer, Philos. Trans. R. Soc. London, Ser. A **260**, 395 (1966).
[43] M. Eidelsberg, J. J. Benayoun, Y. Viala, and F. Rostas, Astron. Astrophys., Suppl. Ser. **90**, 231 (1991).
[44] P. F. Levelt, W. Ubachs, and W. Hogervorst, J. Phys. II France **2**, 801 (1992).
[45] S. Sekine, S. Iwata, and C. Hirose, Chem. Phys. Lett. **180**, 173 (1991).
[46] M. Drabbels, J. Heinze, J. J. ter Meulen, and W. L. Meerts, J. Chem. Phys. **99**, 5701 (1993).
[47] W. Ubachs, K. S. E. Eikema, and W. Hogervorst, J. Opt. Soc. Am. B **14**, 2469 (1997).
[48] P. Cacciani, F. Brandi, J. P. Sprengers, A. Johansson, A. L'Huillier, C.-G. Wahlström, and W. Ubachs, Chem. Phys. **282**, 63 (2002).
[49] K. S. E. Eikema, W. Hogervorst, and W. Ubachs, J. Mol. Spectrosc. **163**, 19 (1994).
[50] K. P. Huber, Philos. Trans. R. Soc. London, Ser. A **355**, 1527 (1997).
[51] J. K. G. Watson, Mol. Phys. **81**, 277 (1994).
[52] H. Lavendy, J. M. Robbe, and J. P. Flament, Chem. Phys. Lett. **205**, 456 (1993).